

Micro-Structural Design of Soft Solid Composite Electrolytes with Enhanced Ionic
Conductivity

by

Nastaran Khodabandehloo

A dissertation submitted to the Department of Mechanical Engineering,
Cullen College of Engineering
in partial fulfillment of the requirements for the degree of

Master of Sciences
in Mechanical Engineering

Chair of Committee: Pradeep Sharma, Professor

Committee Member: Yashashree Kulkarni, Professor

Committee Member: Vedhus Hoskere, Assistant Professor

University of Houston

December 2021

Copyright 2021, Nastaran Khodabandehloo

Abstract

Electrolyte in a rechargeable Li-ion battery plays a critical role in determining its capacity and efficiency. While the typically used electrolytes in Li-ion batteries are liquid, soft solid electrolytes are being increasingly explored as an alternative due to their advantages in terms of increased stability, safety and potential applications in the context of flexible and stretchable electronics. However, ionic conductivity of solid polymer electrolytes is significantly lower compared to liquid electrolytes. In a recent work, we developed a theoretical framework to model the coupled deformation, electrostatics and diffusion in heterogeneous electrolytes and also established a simple homogenization approach for the design of microstructures to enhance ionic conductivity of composite solid electrolytes. Guided by the insights from the theoretical framework, in this paper, we examine specific microstructures that can potentially yield significant improvement in the effective ionic conductivity. We numerically implement our theory in the open source general purpose finite element package *FEniCS* to solve the governing equations and present numerical solutions and insights on the effect of microstructure on the enhancement of ionic conductivity. Specifically, we investigate the effect of shape by considering ellipsoidal inclusions. We also propose an easily manufacturable microstructure that increases the ionic conductivity of the composite electrolyte by forty times, simply by the addition of dielectric columns parallel to the solid electrolyte phase.

Table of Contents

Abstract	iii
Table of Contents	iv
List of Figures	v
1 Introduction	1
2 Theoretical Formulation	5
3 Finite Element Analysis Procedure	12
3.0.1 3.1. Dimensionless form of the governing equations	12
3.0.2 3.2. Weak form	13
3.0.3 3.3. Implementation in <i>FEniCS</i>	15
4 Benchmark Solutions	16
4.1 Uniform electrolyte	16
4.2 Multi-layer composite solid electrolyte	17
5 Results and Discussion	20
5.1 Heterogeneous Electrolytes with Ellipsoidal Inclusions–Shape Effects	20
5.2 Effect of Deformation on Ionic Conductivity of an Electrolyte	27
5.3 A Proposal for a Microstructure to Enhance Ionic Conductivity: Columnar Dielectric Spacers	29
6 Concluding remarks	31
References	32
Appendices	38

List of Figures

1.1	Schematic of the spherulite structure. Reprinted from [1], with the permission of AIP Publishing.	2
2.1	An ionic-conductive electro-elastic-diffusive body in reference and current configuration.	5
4.1	Schematic of a system of uniform electrolyte and electrodes in a battery. . .	16
4.2	Normalized chemical potential across the normalized thickness of rectangular uniform unit cell material.	17
4.3	Schematic of a multi-layer composite electrolyte consisting of a filler, an interphase and a polymer.	18
4.4	Normalized effective ionic conductivity with respect to the volume fraction of the filler for different interphase extension factor(α).	18
5.1	Schematic of an embedded elliptical inclusion.	20
5.2	Normalized ionic conductivity with respect to the volume fraction of the filler for different interphase extension factors(α).	21
5.3	Schematic of a square unit cell matrix with an embedded circular filler with $\alpha = 1$ and a) $\nu_f = 0.78$ b) $\nu_f = 0.43$ and c) $\nu_f = 0.12$ where the light blue, dark blue and yellow colors represent the filler, interphase and polymer respectively.	22
5.4	Chemical potential contour for a square unit cell matrix with an embedded circular filler inclusion for $\alpha = 1$ with different values for volume fraction (a) $\nu_f = 0.78$ (b) $\nu_f = 0.43$ and (c) $\nu_f = 0.12$	23
5.5	Electric potential contour for a square unit cell matrix with an embedded circular filler inclusion for $\alpha = 1$ with different values for volume fraction (a) $\nu_f = 0.78$ (b) $\nu_f = 0.43$ and (c) $\nu_f = 0.12$	23

5.6	Concentration contour for a square unit cell matrix with an embedded circular filler inclusion for $\alpha = 1$ with different values for volume fraction (a) $\nu_f = 0.78$ (b) $\nu_f = 0.43$ and (c) $\nu_f = 0.12$	23
5.7	Normalized ionic conductivity versus the normalized radius of the circular inclusion in a constant volume fraction ($\nu_f = 0.2$) for different interphase thickness (t_{int}) from 0 to 2nm which is normalized with debye length ($\lambda_r = 4\text{nm}$).	24
5.8	Normalized ionic conductivity with respect to the volume fraction of the elliptical filler for different interphase extension factors(α).	25
5.9	Schematics of a square unit cell matrix with an embedded elliptical inclusion with $\alpha = 1$ different $\frac{a}{b}$ (a)0.25 (b)0.5 (c)1 (d)1.5 (e)3.5	26
5.10	Normalized ionic conductivity with respect to $\frac{a}{b}$ for different interphase extension factor α . The ionic conductivity is normalized with the case of the $\alpha = 0$ and $\frac{a}{b} = 0.2$	27
5.11	Schematic of a unit cell under a stretch of ϵ	27
5.12	Normalized ionic conductivity versus average strain for different interphase extension factors α . The ionic conductivity is normalized with the case of the homogeneous system.	28
5.13	Schematic of a battery with an electrolyte and columnar dielectric spacers.	29
5.14	Normalized ionic conductivity with respect to the volume fraction of dielectric. $\frac{\gamma^{\text{dielectric}}}{\gamma^{\text{electrolyte}}} \approx 0$ the initial ionic concentration of the dielectric is considered as zero ($c_0^{\text{dielectric}} = 0$) while for electrolyte we have $c_0^{\text{electrolyte}} = 100 \frac{\text{mol}}{\text{m}^3}$	30

Chapter 1

Introduction

Rechargeable Li-ion batteries are expected to play a central role in the future of energy storage—be it in the context of consumer electronics or sustainable vehicles [2, 3]. The ramifications (and need) for renewable energy, and the critical role energy storage will play in that context, hardly needs much discussion due to the extensive public discourse on the topic and extensive scientific research [4, 5]. Germane to this, scientific research has focused on both fundamental science as well as the designing the relevant materials and motifs to engineer efficient, higher energy density, and safer batteries [6, 7, 8].

A typical Li-ion battery consists of several electrochemical cells connected in series or in parallel. The three primary components of the cell are a negatively charged electrode (cathode), its counterpart—the anode, and an intervening electrolyte that enables ion transfer between the two electrodes. The ionic conductivity of an electrolyte quantifies how mobile and available the ions are in an electrolyte [9], and in addition to other aspects such as the design and chemistry of the electrodes, plays a critical role in the determination of the power output of the cell [10]. An electrolyte should ideally be both an excellent ionic conductor *and* electronic insulator, so that ion transport can be facile and self-discharge is kept to a minimum [11].

Conventionally, electrolytes are liquid. However, increasingly, solid electrolytes are being considered as alternatives. Liquid electrolytes are extremely flammable and a battery containing liquid electrolyte can be fire hazard in case of over-charging or short-circuiting [12]. In contrast, solid electrolytes are thermally stable. Furthermore, liquid electrolytes exhibit a greater propensity for uncontrollable dendritic growth [13] which can cause short circuit conditions[14]. Finally, due to the growing interest in stretchable and flexible electronics, there is a strong impetus to develop soft solid electrolytes that can integrate with such electronic devices [15, 16, 17, 18, 19].

Despite all the advantages that soft (polymer-based) solid electrolytes offer, their ionic conductivity is significantly lower than their widely used liquid counterparts[20]. To that end, several approaches have been proposed to increase the ionic conductivity in polymer electrolytes¹. As an example, a common method to ameliorate ionic conductance is the addition of plasticizers which reduces the crystalline nature of the polymer matrix and can increase the ion mobility of the structure [21]. However mechanical properties may be compromised (i.e. mechanical stability) [22].

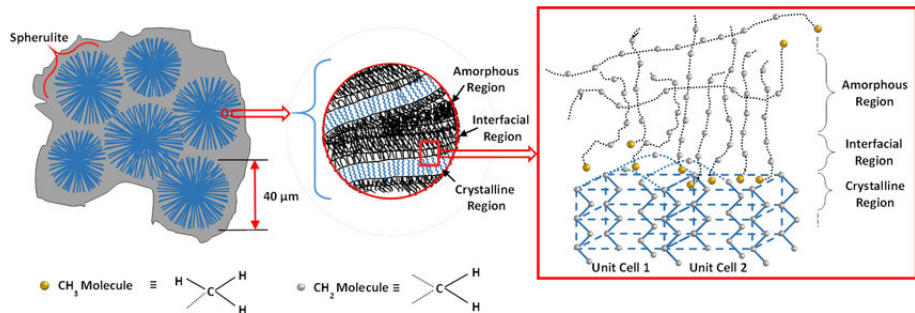


Figure 1.1: Schematic of the spherulite structure. Reprinted from [1], with the permission of AIP Publishing.

Another strategy involves creating composite electrolytes by embedding nanofillers in a polymer matrix [23, 21, 24, 25]. Using such an approach, Croce and co-workers demonstrated a significant enhancement in ionic conductivity [26]. Interestingly, have also shown a *decrease* in ionic conductivity with the addition of nanofillers—e.g. Weston and Steele reported no effect in ionic conductivity by addition of Al₂O₃ and even reduction in ionic conductivity at high volume fractions [27]. The enhancement of ionic conductivity because of addition of nanofillers was attributed to the formation of a spherulite structure in the interphase region of the matrix-inclusion which consists of both highly crystalline structure and amorphous region (as shown in Figure 1.1). This region possesses a much higher ion mobility compared to the polymer electrolyte [28]. Recent studies have also shown that the addition of nano-scale highly-conductive inorganic particulate fillers into polymer electrolytes can not only significantly enhance the ionic conductivity of the electrolytes, but also

¹Ionic conductivity is not the only feature of the electrolyte that is important to battery effectiveness. The operating voltage range, thermal stability among others aspects are also interest. Our work, however, is primarily focused on the improvement of ionic conductivity.

improve its mechanical strength and stability[29]. Finally, mechanical deformation has also been found to strongly influence ionic conductivity of polymer electrolytes [30, 31, 17]. A linear relation between ionic conductivity was found by [31] (for up to 15% strain leading to 400 % improvement in ionic conductivity). This was confirmed by our previous theoretical work [32] predicated on small-deformation theory.

Complementary to experimental efforts (–some of which we have cited in the preceding paragraphs), several theoretical and computational works have also appeared to study the coupled effect of deformation, ionic diffusion and electrostatics. Specifically in the mechanics community, different groups have approached the theory of electrolytes in slightly different manners and often with a different emphasis, or even for applications other than batteries (e.g. ferroelectrics, polymer-metal actuators) [33, 34, 35, 36, 37, 38, 39, 40, 41]. The first paper (that we know of) which proposed homogenization to design composite electrolytes specific to the context of batteries is arguably that of Sillamoni and Idiart (2015) [42]. Very recently, we also proposed [32] a theoretical framework to address the coupling of electrostatics, ionic diffusion and deformation in composite electrolytes. In particular, we presented a simple homogenization procedure that allows the simplification of the rather complicated nonlinear problem and reconciled the various experimental observations in the literature. In our prior work, our approach was almost entirely analytical which limited our modeling to simple microstructures. Guided and inspired by the insights of our prior work, in this paper, we undertake a computational study to understand the effect of some specific microstructures on the possibility of designing enhanced ionic conductivity. Specifically, (i) we implement the pertinent governing equations in the open-source code of *FEniCS*; (ii) analyze composite electrolytes with ellipsoidal inclusions to understand the effect of shape effects on ion conductivity enhancement; (iii) analyze the effect of size of embedded inclusions; (iv) determine the effect of finite deformation on the effective ionic conductivity of electrolytes—our prior work, due to its analytical nature, focused on small-deformation, and (v) propose a specific, easily manufacturable, microstructure that can yield a significant enhancement in ionic conductivity.

This paper is organized as follows, in chapter 2 we briefly summarize the theoretical framework. In chapter 3 we present the relevant details related to our computational

procedure. The primary numerical results for validation are presented in chapter 4 and numerical results for the shape effects and some novel structures are discussed in chapter 5. We conclude in chapter 6.

Chapter 2

Theoretical Formulation

In this section, we briefly summarize the mathematical model of an electro-elastic-diffusive system in an electrolyte we presented in [32].

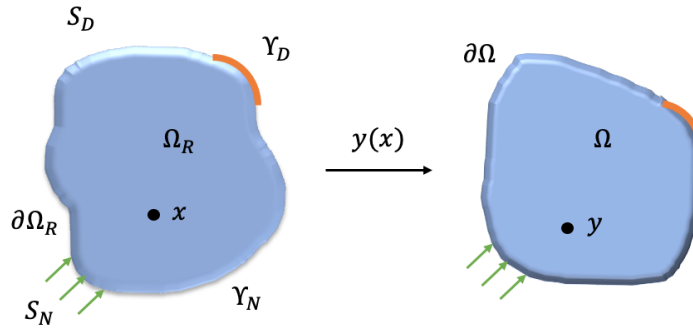


Figure 2.1: An ionic-conductive electro-elastic-diffusive body in reference and current configuration.

Consider Figure 2.1, where we assume that the thermodynamic state of the system is described by deformation $y(0, t) : \Omega_R \rightarrow \Omega(t)$, ionic volumetric concentration $c(0, t) : \Omega_R \rightarrow \mathbb{R}$ and the electric potential $\xi : \Omega_R \rightarrow \mathbb{R}$ in the reference configuration. The deformation gradient, Cauchy-Green tensor, and the Jacobian are denoted by

$$\mathbf{F} = \nabla \mathbf{y}, \quad \mathbf{C} = \mathbf{F}^T \mathbf{F}, \quad \text{and} \quad J = \det \nabla \mathbf{y}. \quad (2.1)$$

Work can be done on the chemo-mechanical-electrical system body through the following boundary conditions:

- Mechanical boundary conditions,

$$\begin{cases} \mathbf{y}(\mathbf{x}, t) = \mathbf{y}_b(\mathbf{x}, t) & \text{on } S_D, \\ \text{applied external traction} = \mathbf{t}^e(\mathbf{x}, t) & \text{on } S_N, \end{cases} \quad (2.2)$$

where $\mathbf{y}_b(0, t) : S_D \rightarrow \mathbb{R}^3$ is the prescribed boundary position and S_D and S_N (as shown in Figure 2.1) are the subdivisions of $\partial\Omega$.

- Electrical boundary condition,

$$\xi = \xi^e(\mathbf{x}) \quad \text{on } \partial\Omega_R, \quad (2.3)$$

where $\xi^e(\mathbf{x})$ is prescribed boundary electric potential on $\partial\Omega_R$ which is controlled by an external circuit.

- Chemical boundary conditions,

$$\begin{cases} \mu = \mu^e(\mathbf{x}, t) & \text{on } \Upsilon_D, \\ \mathbf{J} \cdot \mathbf{n} = \mathbf{J}^e & \text{on } \Upsilon_N, \end{cases} \quad (2.4)$$

where $\mu^e(0, t) : \Upsilon_D \rightarrow \mathbb{R}$ is the prescribed boundary chemical potential which is usually dictated by the materials of active electrodes, and $\mathbf{J}(0, t) : \Omega_R \rightarrow \mathbb{R}^3$ is the ionic flux. Also Υ_D and Υ_N are another subdivisions of $\partial\Omega$.

By the conservation law of ions we have,

$$\dot{c} + \nabla \cdot \mathbf{J} = 0 \quad \text{in } \Omega_R. \quad (2.5)$$

The external system do work on the body by mechanical traction, transportation of ions across the boundary and the applied electric voltage from the electrodes. The rate of work done on the continuum body is

$$\dot{W} = \int_{\partial\Omega_R} \dot{\mathbf{y}} \cdot \mathbf{t}^e - \int_{\partial\Omega_R} (\mu_e + q\xi_e)(\mathbf{J} \cdot \mathbf{n}) - \int_{\partial\Omega_R} \xi(\dot{\tilde{\mathbf{D}}} \cdot \mathbf{n}), \quad (2.6)$$

where q is the electric charge associated with each mobile ion and as a result the electric current density is given by $\mathbf{J}_e = q\mathbf{J}$ [32]. Also $\tilde{\mathbf{D}} = -\epsilon(\mathbf{x})\mathbf{J}\mathbf{C}^{-1}\nabla\xi$ is the nominal electric displacement¹.

¹We remark that the presence of charge diffusion in a continuum body also relates to the so-called electret materials except that in the latter, the charges are “frozen” and convect with deformation in the time-scale

To achieve a closed differential system governing the electro-elastic-diffusion of the body we need to define the free energy of the body through the hypotheses concerning the behavior of the body in equilibrium and non-equilibrium states.

In equilibrium states the free energy of the body is assumed by the function

$$\begin{aligned} U(\mathbf{y}, c) &= U_b(\mathbf{y}, c) + U_e, \\ \text{and } U_b(\mathbf{y}, c) &= \int_{\Omega_R} \Psi(\nabla \mathbf{y}, c), \end{aligned} \quad (2.7)$$

where $\Psi : \mathbb{R}^{3 \times 3} \times \mathbb{R} \rightarrow \mathbb{R}$ is the free energy density and U_e is the electric energy associated with charges and polarization. For simplicity we assume that the material is isotropic so the rate of change of free energy of the body in isothermal process is given by

$$\dot{U}_b = \frac{d}{dt} \int_{\Omega_R} \Psi(\nabla \mathbf{y}, c) = \int_{\Omega_R} \left[\frac{\partial \Psi(\mathbf{F}, c)}{\partial \mathbf{F}} \cdot \nabla \dot{\mathbf{y}} + \frac{\partial \Psi(\mathbf{F}, c)}{\partial c} \dot{c} \right]. \quad (2.8)$$

For brevity we define the following terms,

$$\begin{aligned} \mathbf{P} &:= D_{\mathbf{F}} \Psi(\nabla \mathbf{y}, c) = \frac{\partial \Psi(\mathbf{F}, c)}{\partial \mathbf{F}}, \\ \text{and } \mu &:= D_c \Psi(\nabla \mathbf{y}, c) = \frac{\partial \Psi(\mathbf{F}, c)}{\partial c}. \end{aligned} \quad (2.9)$$

By substituting them in (2.8) and using conservation law of ions presented in (2.5) we rewrite the equation as follows

$$\dot{U}_b = \int_{\Omega_R} [\mathbf{P} \cdot \nabla \dot{\mathbf{y}} - \mu \nabla \cdot \mathbf{J}]. \quad (2.10)$$

As mentioned in (2.7) it is necessary to include the electrical energy associated with the polarization and electric field generated by mobile ions. By neglecting dynamical effects the electric field in reference configuration satisfies Maxwell equation

$$\operatorname{div} \tilde{\mathbf{D}} = \operatorname{div}(-\epsilon(\mathbf{x}) \mathbf{J} \mathbf{C}^{-1} \nabla \xi) = q(c - c_0(\mathbf{x})) \quad \text{in } \Omega_R, \quad (2.11)$$

where $\epsilon(\mathbf{x})$ is the electric permittivity and $c_0 : \Omega_R \rightarrow \mathbb{R}$ is the immobile ion concentration that would neutralize the mobile ions in a natural equilibrium state. For simplicity also we

of interest [43, 44]

assume that the electric permittivity is independent of deformation. Therefore polarization in current configuration can be defined by $\mathbf{p} = -(\epsilon - \epsilon_0)\nabla_{\mathbf{y}}\xi$ in which ϵ_0 is the vacuum permittivity. Hence, the electrical energy stored in the system (U_e) is defined as follows,

$$U_e[\mathbf{y}, c] = \int_{\Omega_R} \left[\frac{\epsilon_0}{2} |\nabla_{\mathbf{y}}\xi|^2 + \frac{|\mathbf{p}|^2}{2(\epsilon(\mathbf{x}) - \epsilon_0)} \right]. \quad (2.12)$$

With a bit of technical calculation the final form of rate of change of electrical energy (U_e) [33], can be written as

$$\dot{U}_e[\mathbf{y}, c] = \int_{\Omega_R} [-\dot{\mathbf{y}} \cdot \text{div} \boldsymbol{\Sigma}_{MW} + \mathbf{J} \cdot \nabla(q\xi)] + \int_{\Omega_R} \dot{\mathbf{y}} \cdot (\boldsymbol{\Sigma}_{MW})\mathbf{n}, \quad (2.13)$$

where $\boldsymbol{\Sigma}_{MW}$ is identified as the Piola-Maxwell stress and is denoted as

$$\boldsymbol{\Sigma}_{MW}(\mathbf{x}) = -\frac{\epsilon(\mathbf{x})}{2} J |\mathbf{F}^{-T} \nabla \xi|^2 \mathbf{F}^{-T} + \epsilon(\mathbf{x}) J (\mathbf{F}^{-T} \nabla \xi) \otimes (\mathbf{F}^{-T} \nabla \xi). \quad (2.14)$$

From (2.6), (2.10) and (2.13) The rate of energy dissipation is written as

$$\begin{aligned} \dot{D} &= \dot{W} - \dot{U} = \dot{W} - \dot{U}_b - \dot{U}_e = \\ & \int_{\partial\Omega_R} \dot{\mathbf{y}} \cdot \mathbf{t}^e - \int_{\partial\Omega_R} (\mu_e + q\xi_e)(\mathbf{J} \cdot \mathbf{n}) \\ & + \int_{\Omega_R} [\text{div}(\mathbf{P} + \boldsymbol{\Sigma}_{MW}) \cdot \dot{\mathbf{y}} - \mathbf{J} \nabla \cdot (\mu + q\xi)] \\ & + \int_{\partial\Omega_R} [-\dot{\mathbf{y}} \cdot (\mathbf{P} + \boldsymbol{\Sigma}_{MW})\mathbf{n} + (\mathbf{J} \cdot \mathbf{n})(\mu + q\xi)] \geq 0. \end{aligned} \quad (2.15)$$

The inequality is from the 2nd law of thermodynamics—the rate of energy dissipation must always be a positive value ($\dot{D} \geq 0$).

Using the standard Coleman-Noll procedure the following arguments can be concluded:

- Non-negative rate of dissipation

$$-\mathbf{J} \cdot \nabla(\mu + q\xi) \geq 0. \quad (2.16)$$

- Interior mechanical balance

$$\operatorname{div}(\mathbf{P} + \boldsymbol{\Sigma}_{MW}) = 0 \quad \text{in } \Omega_R. \quad (2.17)$$

- Boundary conditions

$$(\mathbf{P} + \boldsymbol{\Sigma}_{MW})\mathbf{n} - \mathbf{t}^e = 0 \quad \text{on } S_N, \quad (2.18)$$

and

$$\begin{cases} \mu^e + q\xi^e = \mu + q\xi & \text{on } \Upsilon_D, \\ \mathbf{J} \cdot \mathbf{n} = 0 & \text{on } \Omega_R \setminus \Upsilon_D. \end{cases} \quad (2.19)$$

By (2.16) a constitutive response that is consistent with the second law of thermodynamics which represents the simplest choice is the linear mobility/diffusion,

$$\mathbf{v} = -\gamma(\mathbf{x})\nabla(\mu + q\xi), \quad \mathbf{J} = c\mathbf{v} \quad \text{in } \Omega_R, \quad (2.20)$$

where $\gamma(\mathbf{x})$ represents the ionic mobility of the material which depends on the position.

In this work, we will consider both finite and infinitesimal deformation to understand not only the effect of deformation but also the importance (or not) of accounting for large deformation behavior. For a linearized theory we expand the free energy density at a reference equilibrium state as follows,

$$\begin{aligned} \Psi(\mathbf{F}, c; \mathbf{x}) &\approx \frac{1}{2}(\mathbf{F} - \mathbf{I}) \cdot \mathbb{C}(\mathbf{x})(\mathbf{F} - \mathbf{I}) + \alpha_{\text{el}}(c - c_0(\mathbf{x}))\operatorname{Tr}(\mathbf{F} - \mathbf{I}) \\ &+ \frac{\beta(\mathbf{x})}{2}(c - c_0(\mathbf{x}))^2 + \hat{\mu}(\mathbf{x})(c - c_0(\mathbf{x})) + \Psi(\mathbf{I}, c_0; \mathbf{x}), \end{aligned} \quad (2.21)$$

where \mathbf{I} is the identity matrix, and $\hat{\mu}$ denotes the chemical potential for pure ion, and \mathbb{C} is the forth-order elasticity tensor.

In the case of infinitesimal deformation, the complete coupled system of governing equations for (μ, ξ, \mathbf{u}) using (2.21) can now be written as

$$\left\{ \begin{array}{l} \nabla \cdot (-\epsilon_r \nabla \xi) + \frac{q^2}{\epsilon_0 \beta} \xi = \frac{q}{\epsilon_0 \beta} (\mu + q\xi - \hat{\mu} - \alpha_{\text{el}} \nabla \cdot \mathbf{u}) \quad \text{in } \Omega_R, \\ \nabla \cdot [\mathbb{C} \nabla \mathbf{u} + \frac{\alpha_{\text{el}}}{\beta} (\mu - \hat{\mu} - \alpha_{\text{el}} \nabla \cdot \mathbf{u}) \mathbf{I}] = 0 \quad \text{in } \Omega_R, \\ \nabla \cdot [(-\gamma c \nabla (\mu + q\xi))] = \dot{c}, \quad c - c_0 = \frac{(\mu - \hat{\mu} - \alpha_{\text{el}} \nabla \cdot \mathbf{u})}{\beta} \quad \text{in } \Omega_R. \end{array} \right. \quad (2.22)$$

To account deformation nonlinearity, we will consider an incompressible neo-Hookean material. However, we also note that the permeation of charged ions (or uncharged molecules) induces significant volume change of the material. To model this phenomenon, we may enforce a kinematic constraint

$$\Phi(\mathbf{F}, c) = \det \mathbf{F} - (1 + \nu_i (c - c_0)) = 0, \quad (2.23)$$

where ν_i can be interpreted as volume of ions [32]. Accounting for the constraint, the free energy density of the body Ω_R can be written as

$$\Psi(\mathbf{F}, c) = \frac{1}{2} G (|\mathbf{F}|^2 - 3) + \frac{\beta}{2} (c - c_0)^2 + \hat{\mu} (c - c_0) - \Pi \Phi(\mathbf{F}, c), \quad (2.24)$$

where G is the shear modulus. So the governing equations then become

$$\left\{ \begin{array}{l} \nabla \cdot (-\epsilon_r \nabla \xi) + \frac{q^2}{\epsilon_0 \beta} \xi = \frac{q}{\epsilon_0 \beta} (\mu + q\xi - \hat{\mu} - \Pi \nu_i) \quad \text{in } \Omega_R, \\ \nabla \cdot [\mathbf{P} + \Sigma_{MW}] = 0 \quad \text{in } \Omega_R, \\ \nabla \cdot [(-\gamma c \nabla (\mu + q\xi))] = \dot{c}, \quad c - c_0 = \frac{(\mu - \hat{\mu} - \Pi \nu_i)}{\beta} \quad \text{in } \Omega_R, \end{array} \right. \quad (2.25)$$

where $\mathbf{P} = G\mathbf{F} - J\Pi\mathbf{F}^{-T}$.

To demonstrate the fundamental behavior of the system in (2.22) and (2.25) and analyze the homogenization of composite electrolytes, we consider a one-dimensional and homogeneous electrolyte body between two charge collectors $\Delta\xi = \xi_1 - \xi_0$. We also introduce electro-chemical potential,

$$\Phi = \mu + q\xi, \quad (2.26)$$

and Debye length as the screening length for electrostatic interactions ²,

$$\lambda = \sqrt{\frac{\epsilon_0 \beta}{q^2}}. \quad (2.27)$$

Taking cognizance of the relation between the ionic flux J and the external electrical current $I = qJA$, the ionic conductivity of electrolyte must satisfy equation,

$$J = -K \frac{\Delta \phi}{d}, \quad (2.28)$$

where ϕ is the electro-chemical potential and defined as $\phi = \mu + q\xi$ [32]. The electric potential difference between the electrodes satisfies Ohm's law $\Delta \xi = IR = qJAR$.

To facilitate the interpretation of ionic conductivity, consider one-dimensional ion transport in non-equilibrium process where $J \neq 0$ which is the steady-state limit of (2.22). In that case, we have the following relation for electrochemical potential difference,

$$\Delta \phi = \phi_1 - \phi_0 = -\frac{Jd}{K} = -\int_0^d \frac{J}{\gamma c(x)} dx = -\int_0^d \frac{J}{\gamma(c + \hat{c})} dx, \quad (2.29)$$

where \hat{c} is the change of concentration due to ion transportation. Assuming the change of concentration of ions is mostly due to the chemical potential difference in the boundaries [32], we can safely neglect \hat{c} and rewrite (2.29) as below,

$$\phi' = \frac{J}{\gamma(c + \hat{c})} \approx \frac{J}{\gamma c} \rightarrow \Delta \phi \approx -J \int_0^d \frac{1}{\gamma c(x)} dx. \quad (2.30)$$

Therefore using (2.28) the ionic conductivity K in one-dimension can be defined as

$$K = \left[\frac{1}{d} \int_0^d \frac{1}{\gamma c(x)} dx \right]^{-1}, \quad (2.31)$$

where $c(x)$ is the equilibrium ionic concentration obtained from solving (2.22) in steady state equilibrium condition.

²The *conventional* homogenization the conductivity problem (predicated on the classical Poisson equation) is size-independent. However, in the current framework, due to the presence of the Debye length, there is a characteristic length scale that renders the ionic conductivity dependent on the length-scale of the microstructure. This is reminiscent of surface energy effects [45, 46, 47] or gradient-type continuum theories [48, 49].

Chapter 3

Finite Element Analysis Procedure

The governing partial differential equations for the chemo-electro-mechanical system derived in the preceding section are very difficult to solve but for some very simple cases. In this section, we described the finite element implementation to solve these numerically.

3.0.1 3.1. Dimensionless form of the governing equations

As a first step to derive the corresponding weak form of the coupled system of partial differential equations, we non-dimensionalize them to simplify the calculations and facilitate eventual physical interpretation. As evident, three primary variables are involved (ξ , μ , \mathbf{u}) denotes for the electric potential scalar field, chemical potential scalar field and displacement vector field. The dimensionless parameters and the dimensionless constant coefficients are presented below,

$$\begin{aligned}
 \bar{\xi} &= \frac{\xi q}{\mu_{\text{ref}}}, & \bar{\mathbf{u}} &= \frac{\mathbf{u}}{H}, & \bar{\mu} &= \frac{\mu}{\mu_{\text{ref}}}, & \bar{c} &= \frac{c}{c_{\text{ref}}}, \\
 \bar{t} &= \frac{t}{T}, & (T &= \frac{\mu_{\text{ref}} \gamma_{\text{ref}}}{H^2}), \\
 \bar{\beta} &= \frac{\beta c_{\text{ref}}^2}{G_{\text{ref}}}, & \bar{\hat{\mu}} &= \frac{\hat{\mu}}{\mu_{\text{ref}}}, & \bar{c}_0 &= \frac{c_0}{c_{\text{ref}}}, \\
 \bar{\gamma} &= \frac{\gamma}{\gamma_{\text{ref}}}, & \bar{\alpha}_{\text{el}} &= \frac{\alpha_{\text{el}} c_{\text{ref}}}{G_{\text{ref}}}, & \text{and } \bar{\nabla} &= H \nabla,
 \end{aligned} \tag{3.1}$$

where H , T are the non-dimensionalization parameters associated with the smallest length scale and the time scale respectively and G is the shear modulus. Also, c_{ref} , μ_{ref} , G_{ref} and γ_{ref} are the normalization factors associated with the primary variables. For simplicity we set $c_{\text{ref}} = c_0$, $\mu_{\text{ref}} = \hat{\mu}$, $G_{\text{ref}} = G$ and $\gamma_{\text{ref}} = \gamma$ for the homogeneous electrolyte. With this, the governing equations in dimensionless form are

$$\bar{\nabla} \cdot (-\epsilon_r \bar{\nabla} \bar{\xi}) - \frac{\Phi^2}{\bar{\beta}} (\bar{\mu} - \bar{\hat{\mu}}) + \frac{\bar{\alpha}_{\text{el}} \Phi^2}{\bar{\beta}} \frac{\bar{\nabla} \cdot \bar{\mathbf{u}}}{\Gamma} = 0, \tag{3.2}$$

$$\bar{\nabla} \cdot \left[\frac{\mathbb{C}}{G_{\text{ref}}} \bar{\nabla} \bar{\mathbf{u}} + \bar{\alpha}_{\text{el}} \frac{\Gamma}{\beta} (\bar{\mu} - \bar{\hat{\mu}}) \mathbf{I} - \frac{\bar{\alpha}_{\text{el}}^2}{\beta} \bar{\nabla} \cdot \bar{\mathbf{u}} \mathbf{I} \right] = 0, \quad (3.3)$$

and

$$\begin{aligned} \bar{\nabla} \cdot \left[-\bar{\gamma} \left(\frac{\Gamma}{\beta} (\bar{\mu} - \bar{\hat{\mu}}) - \bar{\nabla} \cdot \bar{\mathbf{u}} \frac{\bar{\alpha}_{\text{el}}}{\beta} + \bar{c}_0 \right) \bar{\nabla} (\bar{\mu} + \bar{\xi}) \right] = \\ \frac{H^2}{\mu_{\text{ref}} \gamma_{\text{ref}}} \frac{1}{T} \frac{d}{dt} \left(\frac{\Gamma}{\beta} (\bar{\mu} - \bar{\hat{\mu}}) - \bar{\nabla} \cdot \bar{\mathbf{u}} \frac{\bar{\alpha}_{\text{el}}}{\beta} + \bar{c}_0 \right), \end{aligned} \quad (3.4)$$

where $\Phi = \frac{Hq c_{\text{ref}}}{\sqrt{\epsilon_0} G_{\text{ref}}}$ and $\Gamma = \frac{\mu_{\text{ref}} c_{\text{ref}}}{G_{\text{ref}}}$.

For the neo-Hookean case presented in (2.25), the additional dimensionless parameters are,

$$\bar{\nu}_i = \nu_i c_{\text{ref}}, \quad \bar{\Pi} = \frac{\Pi}{G_{\text{ref}}}. \quad (3.5)$$

The dimensionless form of the governing equations become,

$$\bar{\nabla} \cdot \left(-\epsilon_r \bar{\nabla} \bar{\xi} \right) - \frac{\Phi^2}{\beta} (\bar{\mu} - \bar{\hat{\mu}}) + \frac{\bar{\nu}_i \Phi^2}{\beta \Gamma} \bar{\Pi} = 0, \quad (3.6)$$

$$\bar{\nabla} \cdot \left[\bar{\nabla} \bar{\mathbf{u}} + \mathbf{I} - \det(\bar{\nabla} \bar{\mathbf{u}} + \mathbf{I}) \bar{\Pi} (\bar{\nabla} \bar{\mathbf{u}} + \mathbf{I})^{-\text{T}} \right] = 0, \quad (3.7)$$

and

$$\begin{aligned} \bar{\nabla} \cdot \left[-\bar{\gamma} \left(\frac{\Gamma}{\beta} (\bar{\mu} - \bar{\hat{\mu}}) - \bar{\Pi} \frac{\bar{\nu}_i}{\beta} + \bar{c}_0 \right) \bar{\nabla} (\bar{\mu} + \bar{\xi}) \right] = \\ \frac{H^2}{\mu_{\text{ref}} \gamma_{\text{ref}}} \frac{1}{T} \frac{d}{dt} \left(\frac{\Gamma}{\beta} (\bar{\mu} - \bar{\hat{\mu}}) - \bar{\Pi} \frac{\bar{\nu}_i}{\beta} + \bar{c}_0 \right). \end{aligned} \quad (3.8)$$

3.0.2 3.2. Weak form

We write the weak forms of governing equations by employing three test functions ν , $\boldsymbol{\omega}$ and ρ for the scalar electric potential ξ , displacement vector \mathbf{u} , and the chemical potential μ . By multiplying the governing equations by the test functions, integrating over the volume, and using the divergence theorem, the weak forms can be written as

$$\begin{aligned} & \int_{\partial\Omega} \bar{\nabla} \cdot (-\epsilon_r \bar{\nabla} \bar{\xi}) \nu \cdot \mathbf{n}_i dS - \int_{\Omega} (-\epsilon_r \bar{\nabla} \bar{\xi}) \bar{\nabla} \nu dV \\ & - \int_{\Omega} \left(\frac{\Phi^2}{\beta} (\bar{\mu} - \bar{\hat{\mu}}) \nu + \frac{\bar{\alpha}_{el}}{\beta} \frac{\Phi^2}{\Gamma} \bar{\nabla} \cdot (\bar{\mathbf{u}}) \nu \right) dV = 0, \end{aligned} \quad (3.9)$$

$$\begin{aligned} & \int_{\partial\Omega} \left[\frac{\mathbb{C}}{G_{ref}} \bar{\nabla} \bar{\mathbf{u}} + \bar{\alpha}_{el} \frac{\Gamma}{\beta} (\bar{\mu} - \bar{\hat{\mu}}) \mathbf{I} - \frac{\bar{\alpha}_{el}^2}{\beta} \bar{\nabla} \cdot \bar{\mathbf{u}} \mathbf{I} \right] \boldsymbol{\omega} \cdot \mathbf{n}_i dS \\ & - \int_{\Omega} \left[\frac{\mathbb{C}}{G_{ref}} \bar{\nabla} \bar{\mathbf{u}} + \bar{\alpha}_{el} \frac{\Gamma}{\beta} (\bar{\mu} - \bar{\hat{\mu}}) \mathbf{I} - \frac{\bar{\alpha}_{el}^2}{\beta} \bar{\nabla} \cdot \bar{\mathbf{u}} \mathbf{I} \right] \bar{\nabla} \boldsymbol{\omega} dV = 0, \end{aligned} \quad (3.10)$$

and

$$\begin{aligned} & \int_{\partial\Omega} \left[-\bar{\gamma} \left(\frac{\Gamma}{\beta} (\bar{\mu} - \bar{\hat{\mu}}) - \bar{\nabla} \cdot \bar{\mathbf{u}} \frac{\bar{\alpha}_{el}}{\beta} + \bar{c}_0 \right) \bar{\nabla} (\bar{\mu} + \bar{\xi}) \right] \rho \cdot \mathbf{n}_i dS \\ & - \int_{\Omega} \left[-\bar{\gamma} \left(\frac{\Gamma}{\beta} (\bar{\mu} - \bar{\hat{\mu}}) - \bar{\nabla} \cdot \bar{\mathbf{u}} \frac{\bar{\alpha}_{el}}{\beta} + \bar{c}_0 \right) \bar{\nabla} (\bar{\mu} + \bar{\xi}) \right] \bar{\nabla} \cdot \rho dV = \\ & \int_{\Omega} \frac{H^2}{\mu_{ref} \gamma_{ref}} \frac{1}{T} \frac{d}{dt} \left(\frac{\Gamma}{\beta} (\bar{\mu} - \bar{\hat{\mu}}) - \bar{\nabla} \cdot \bar{\mathbf{u}} \frac{\bar{\alpha}_{el}}{\beta} + \bar{c}_0 \right) \rho dV. \end{aligned} \quad (3.11)$$

Test functions $\boldsymbol{\omega}$, ν , and ρ on the boundary are constrained to be zero as stated below,

$$\boldsymbol{\omega} = \rho = \nu = 0 \quad \text{on } \partial\Omega. \quad (3.12)$$

Using (3.12) the first terms of (3.9),(3.10),(3.11) are equal to zero, as follows,

$$\int_{\partial\Omega} \bar{\nabla} \cdot (-\epsilon_r \bar{\nabla} \bar{\xi}) \nu \cdot \mathbf{n}_i dS = 0, \quad (3.13)$$

$$\int_{\partial\Omega} \left[\frac{\mathbb{C}}{G_{ref}} \bar{\nabla} \bar{\mathbf{u}} + \bar{\alpha}_{el} \frac{\Gamma}{\beta} (\bar{\mu} - \bar{\hat{\mu}}) \mathbf{I} - \frac{\bar{\alpha}_{el}^2}{\beta} \bar{\nabla} \cdot \bar{\mathbf{u}} \mathbf{I} \right] \boldsymbol{\omega} \cdot \mathbf{n}_i dS = 0, \quad (3.14)$$

and

$$\int_{\partial\Omega} \left[-\bar{\gamma} \left(\frac{\Gamma}{\beta} (\bar{\mu} - \bar{\hat{\mu}}) - \bar{\nabla} \cdot \bar{\mathbf{u}} \frac{\bar{\alpha}_{el}}{\beta} + \bar{c}_0 \right) \bar{\nabla} (\bar{\mu} + \bar{\xi}) \right] \rho \cdot \mathbf{n}_i dS = 0. \quad (3.15)$$

Using (3.13), (3.14) and (3.15) equations (3.9),(3.10) and (3.11) will be shorten to the following forms,

$$- \int_{\Omega} (-\epsilon_r \bar{\nabla} \bar{\xi}) \bar{\nabla} \nu dV - \int_{\Omega} \left(\frac{\Phi^2}{\beta} (\bar{\mu} - \bar{\hat{\mu}}) \nu + \frac{\bar{\alpha}_{el}}{\beta} \frac{\Phi^2}{\Gamma} \bar{\nabla} \cdot (\bar{\mathbf{u}}) \nu \right) dV = 0, \quad (3.16)$$

$$\int_{\Omega} \left[\frac{\mathbb{C}}{G_{\text{ref}}} \bar{\nabla} \bar{\mathbf{u}} + \bar{\alpha}_{\text{el}} \frac{\Gamma}{\beta} (\bar{\mu} - \hat{\mu}) \mathbf{I} - \frac{\bar{\alpha}_{\text{el}}^2}{\beta} \bar{\nabla} \cdot \bar{\mathbf{u}} \mathbf{I} \right] \bar{\nabla} \boldsymbol{\omega} dV = 0, \quad (3.17)$$

and

$$\begin{aligned} & - \int_{\Omega} \left[-\bar{\gamma} \left(\frac{\Gamma}{\beta} (\bar{\mu} - \hat{\mu}) - \bar{\nabla} \cdot \bar{\mathbf{u}} \frac{\bar{\alpha}_{\text{el}}}{\beta} + \bar{c}_0 \right) \bar{\nabla} (\bar{\mu} + \bar{\xi}) \right] \bar{\nabla} \cdot \rho dV = \\ & \int_{\Omega} \frac{H^2}{\mu_{\text{ref}} \gamma_{\text{ref}}} \frac{1}{T} \frac{d}{dt} \left(\frac{\Gamma}{\beta} (\bar{\mu} - \hat{\mu}) - \bar{\nabla} \cdot \bar{\mathbf{u}} \frac{\bar{\alpha}_{\text{el}}}{\beta} + \bar{c}_0 \right) \rho dV. \end{aligned} \quad (3.18)$$

For the system in (2.25), the weak form can be written as follows,

$$- \int_{\Omega} (-\epsilon_r \bar{\nabla} \bar{\xi}) \bar{\nabla} \nu dV - \int_{\Omega} \left(\frac{\Phi^2}{\beta} (\bar{\mu} - \hat{\mu}) \nu + \frac{\bar{\nu}_i}{\beta} \frac{\Phi^2}{\Gamma} \bar{\Pi} \right) \nu dV = 0, \quad (3.19)$$

$$\int_{\Omega} [\bar{\nabla} \bar{\mathbf{u}} + \mathbf{I} - \det(\bar{\nabla} \bar{\mathbf{u}} + \mathbf{I}) \bar{\Pi} (\bar{\nabla} \bar{\mathbf{u}} + \mathbf{I})^{-T}] \bar{\nabla} \boldsymbol{\omega} dV = 0, \quad (3.20)$$

and

$$\begin{aligned} & - \int_{\Omega} \left[-\bar{\gamma} \left(\frac{\Gamma}{\beta} (\bar{\mu} - \hat{\mu}) - \bar{\Pi} \frac{\bar{\nu}_i}{\beta} + \bar{c}_0 \right) \bar{\nabla} (\bar{\mu} + \bar{\xi}) \right] \bar{\nabla} \cdot \rho dV = \\ & \int_{\Omega} \frac{H^2}{\mu_{\text{ref}} \gamma_{\text{ref}}} \frac{1}{T} \frac{d}{dt} \left(\frac{\Gamma}{\beta} (\bar{\mu} - \hat{\mu}) - \bar{\Pi} \frac{\bar{\nu}_i}{\beta} + \bar{c}_0 \right) \rho dV. \end{aligned} \quad (3.21)$$

3.0.3 3.3. Implementation in *FEniCS*

The governing equations presented in the previous section (in their weak form) are solved using the general-purpose open-source PDE solver *FEniCS*. The weak forms and the corresponding finite element discretization are specified using a domain-specific language, named UFL (Unified Form Language) embedded in Python. The computational domain is partitioned into non-overlapping triangular elements with quadratic interpolation for displacement and linear interpolation for chemical and electric potential in a continuous Galerkin function space. The discrete trial and test spaces are defined by constructing finite element shape functions over the union of all elements in Ω [50].

Chapter 4

Benchmark Solutions

Before proceeding to analyze microstructures that are intractable analytically, to ensure first that our finite element implementation is correct, we compare our numerical results with some known analytical results in different sections for uniform electrolyte and a laminate electrolyte structure.

4.1 Uniform electrolyte

We first analyze the the simplified problem of a one-dimensional and homogeneous electrolyte as shown in the Figure 4.1 with electric potential difference between two charge collectors $\Delta\xi = (\xi_1 - \xi_0)$. Elasticity is decoupled for this illustrative problem so we set $\alpha = 0$. The analytical result for the chemical potential along the thickness of the electrolyte is given by,

$$\mu(x) = \frac{\mu_0 - \eta\mu_d}{1 - \eta^2} e^{-\frac{x}{\lambda_r}} + \frac{-\eta\mu_0 + \mu_d}{1 - \eta^2} e^{\frac{x-d}{\lambda_r}}, \quad (4.1)$$

where λ_r is the Debye length and $\eta = e^{-\frac{d}{\lambda_r}}$ [32]. In Figure 4.2, we contrast the results of our finite element calculation with the closed-form solution.

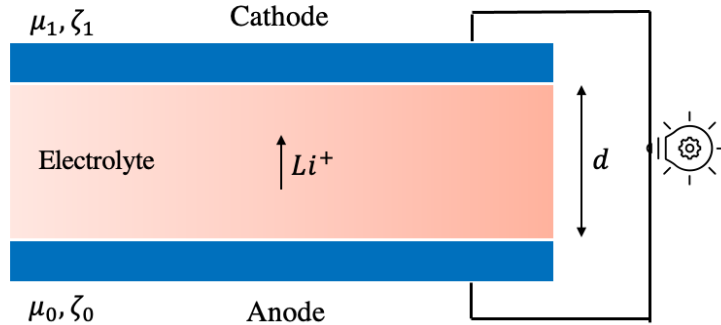


Figure 4.1: Schematic of a system of uniform electrolyte and electrodes in a battery.

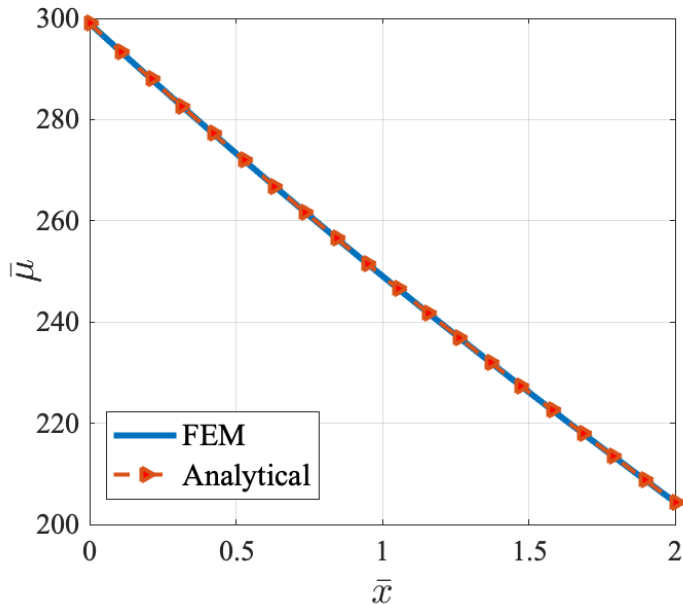


Figure 4.2: Normalized chemical potential across the normalized thickness of rectangular uniform unit cell material.

4.2 Multi-layer composite solid electrolyte

As partially discussed the context of Figure 1.1, past research appears to indicate that addition of nano-particles in a polymer alters the region in the vicinity of the particle thus forming an interphase layer. The interphase layer, while substantively the same as the polymer matrix in physical and mechanical behavior exhibits significantly higher ionic mobility than the polymer[51]. In short, a three-phase composite consisting of an inclusion (typically ceramic), its surrounding matrix (typically soft polymer) and an interphase region, is an adequate description of actual solid composite electrolyte systems. Arguably, the simplest possible composite electrolyte is a multi-layer laminate. The problem essentially becomes one-dimensional in nature. In this section, we benchmark our numerical results for three-layer solid electrolyte laminate structure (Figure 4.3).

Denoting the total thickness of the system by d , we refer to the inclusion, polymer and interphase dimensions as d_p , d_{int} and d_f respectively. We define a constant of proportionality, α , called interphase extension factor, to introduce the normalization of d_{int} with respect to the size of the inclusion as follows,



Figure 4.3: Schematic of a multi-layer composite electrolyte consisting of a filler, an interphase and a polymer.

$$d_{int} = \alpha d_f = \alpha \nu_f d. \quad (4.2)$$

To generate numerical results and study the effect of volume fraction, we fix the inclusion size to a thickness of 2 nm, and vary the thickness of the polymer (d_p). The calculations are performed for different interphase extension factors. We note that the results are *size-dependent* unlike classical conductivity problems.

Figure 4.4 shows the normalized effective ionic conductivity with respect to the volume fraction of the filler $\nu_f = \frac{d_f}{d}$ for different values of α .

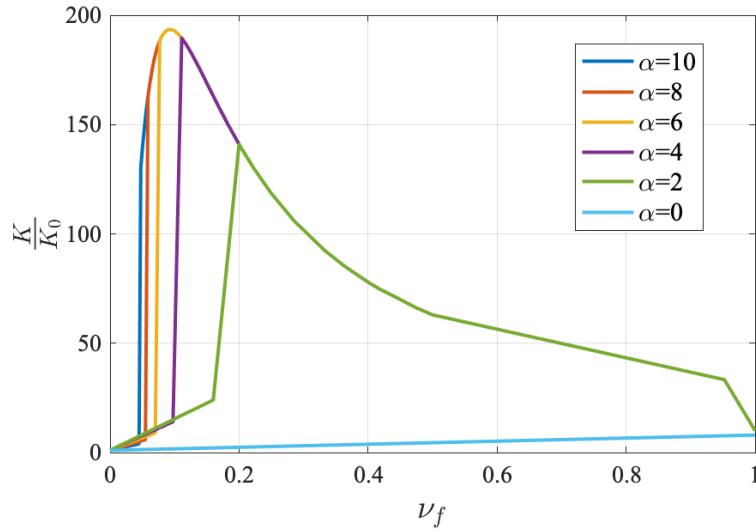


Figure 4.4: Normalized effective ionic conductivity with respect to the volume fraction of the filler for different interphase extension factor (α).

We remark that, K_0 is the ionic conductivity of the case when $\nu_f = 0$. The $\alpha = 0$ corresponds to an absence of an interphase, and as expected, the effective ionic conductivity of

the composite does not vary much with an increase in volume fraction of the inclusion phase. However, when $\alpha > 0$ we see a significant enhancement. This is hardly surprising since the interphase region has been found to be highly conductive and larger this phase, higher the effective ionic conductivity. This corresponds well with the thesis (and experimental observation) that even though second phase particles may not be by themselves ionically conductive, they alter the region around the particles to make it more conductive. In this situation we consider $\gamma^{filler} = \gamma^{polymer} = \frac{\gamma^{interphase}}{1000}$ the initial concentration is considered as zero ($c_0^{filler} = 0$) and for interphase and polymer we have $c_0^{interphase} = c_0^{polymer} = 50 \frac{mol}{m^3}$. The numerical values are $\lambda_r^{interphase} = \lambda_r^{filler} = \lambda_r^{polymer} = 4nm$ and $\epsilon_r^{filler} = 10, \epsilon_r^{polymer} = \epsilon_r^{interphase} = 3, \hat{\mu}^{polymer} = \hat{\mu}^{interphase} = 0.5eV$ and $\hat{\mu}^{polymer} - \hat{\mu}^{filler} = 1eV$.

Chapter 5

Results and Discussion

We now turn to the central results of our paper where we analyze different microstructures that are not amenable to analytical solution.

5.1 Heterogeneous Electrolytes with Ellipsoidal Inclusions—Shape Effects

The ellipsoidal shape allows us to study the effect of particle shape on the effective conductivity enhancement. We remark that this specific insight does not appear to have been discussed in the literature so far.

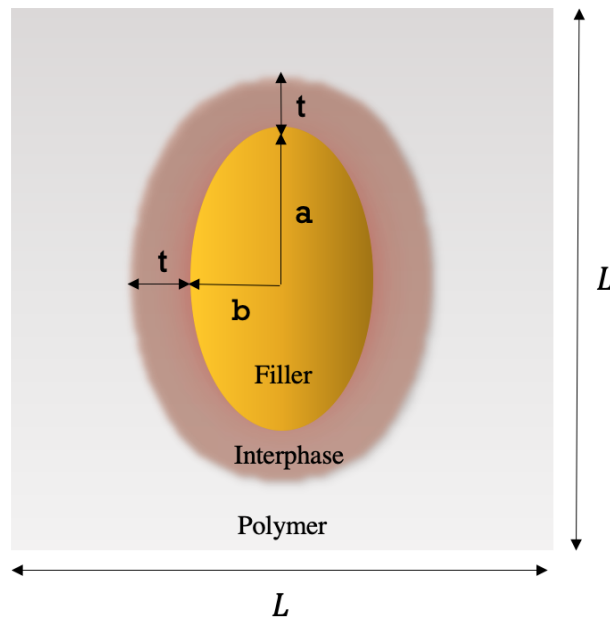


Figure 5.1: Schematic of an embedded elliptical inclusion.

As shown in Figure 5.1, we consider the two-dimensional case of an elliptical inclusion

with the major and minor axes, $2b$ and $2a$ in a square unit cell of polymer matrix (of length L). The interphase of thickness t is assumed to be uniform and we will analyze the steady-state limit of the governing equations.

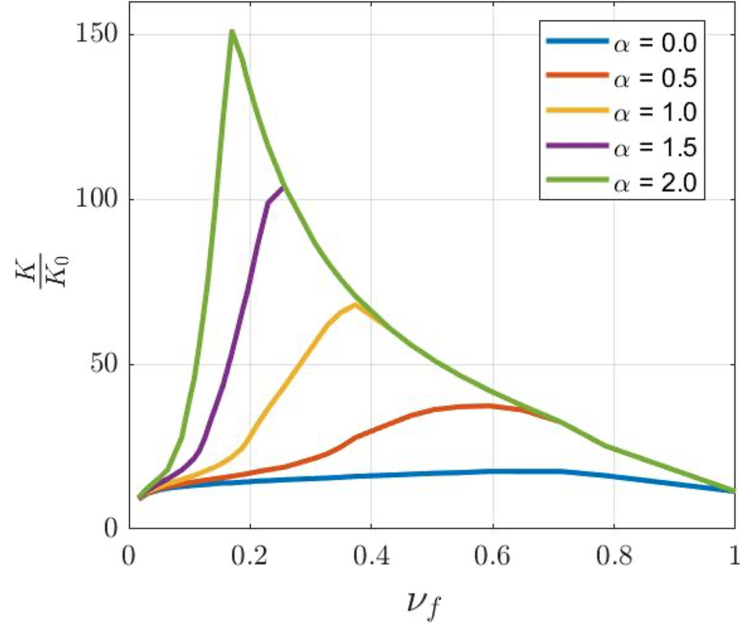


Figure 5.2: Normalized ionic conductivity with respect to the volume fraction of the filler for different interphase extension factors(α).

In what follows, we fix the interphase thickness (t) and vary the interphase extension factor(α) which can be defined as $\alpha = \frac{t}{a}$. We first analyze the simplified case of circular geometry ($a = b$). We remark that the case of a single circular inclusion case can indeed be solved analytically (c.f. [32]) however homogenization can only proceed approximately. Of course, in the case of a general elliptical inclusion neither the problem of a single inclusion nor the homogenization are analytically tractable. For the circular inclusion case study, we fix the size of the particle ($a = b = 1\text{nm}$) and volume fraction is altered by varying L . The unit cell is subject to a constant electric potential difference $\Delta\mu = 200 \times \mu_{\text{ref}} = 100\text{eV}$. In equilibrium state ($\phi = 0$), the $\Delta\xi = -\frac{\Delta\mu}{q} = -100\text{V}$.

Figure 5.2 illustrates the normalized effective ionic conductivity versus volume fraction of an embedded circular filler in a square unit cell. Here, K_0 represents the ionic conductivity of a uniform polymer electrolyte. We observe essentially the same trend as

in Figure 4.4 where the effective ionic conductivity of the composite reaches a maximum point (for some specific volume fraction) and then decreases to its initial value. Consistent with the one-dimensional study in the preceding section, the interphase plays a dominant role and (as example) for $\alpha = 2$ we see that the ionic conductivity enhances by an order of magnitude. For any $\alpha > 0$ the composite reaches its maximum effective ionic conductivity at the point where the interphase reaches its maximum volume fraction in a unit cell.

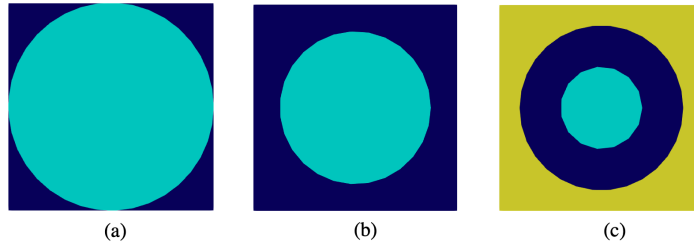


Figure 5.3: Schematic of a square unit cell matrix with an embedded circular filler with $\alpha = 1$ and a) $\nu_f = 0.78$ b) $\nu_f = 0.43$ and c) $\nu_f = 0.12$ where the light blue, dark blue and yellow colors represent the filler, interphase and polymer respectively.

To better illustrate this phenomena, Figure 5.3 presents three different schematics of a square unit cell with an embedded circular filler with $\alpha = 1$ for three different values for volume fractions 0.78, 0.43 and 0.12. Each of these three schematics shows an individual point on the yellow graph in Figure 5.2 where $\alpha = 1$. So if we put Figure 5.2 and the yellow graph in Figure 5.3 together, we are able to see the difference in effective ionic conductivity in different structures. For instance, in Figure 5.3(a), where $\nu_f = 0.78$, the unit cell is filled with filler and interphase but $\frac{K}{K_0} \approx 25$ which is not the maximum value. Moving from $\nu_f = 0.78$ to $\nu_f = 0.43$ (situation illustrated in Figure 5.3(b)) we can see from Figure 5.2 as the volume fraction of the filler decreases and size of interphase increases instead, the effective ionic conductivity of the composite increases until a point from the unit cell in filled with filler and interphase but the interphase has its maximum size. So after reaching the maximum effective ionic conductivity at situation Figure 5.3(b), if we move from Figure 5.3(b) to Figure 5.3(c) where the volume fraction of the filler decreases and the unit cell consists filler, interphase and polymer, according to the yellow graph on Figure 5.2 the $\frac{K}{K_0} \approx 25$ again which means the effective ionic conductivity decreased by addition of extra

polymer in the unit cell. Hence, the maximum effective ionic conductivity in a square unit cell with an embedded circular filler can be reached where the interphase is at its maximum volume fraction.

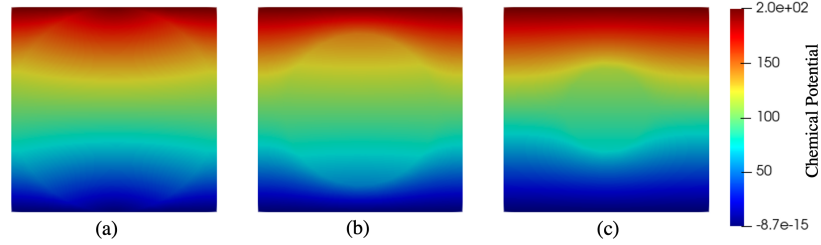


Figure 5.4: Chemical potential contour for a square unit cell matrix with an embedded circular filler inclusion for $\alpha = 1$ with different values for volume fraction (a) $\nu_f = 0.78$ (b) $\nu_f = 0.43$ and (c) $\nu_f = 0.12$

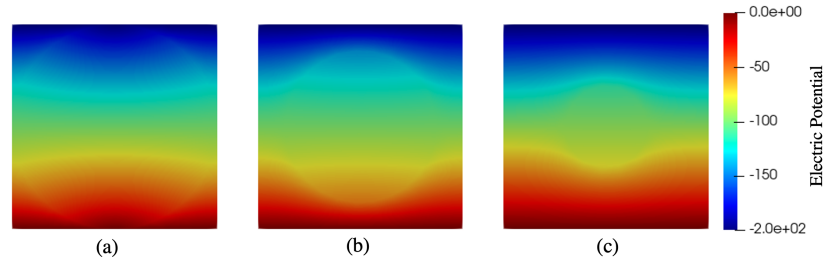


Figure 5.5: Electric potential contour for a square unit cell matrix with an embedded circular filler inclusion for $\alpha = 1$ with different values for volume fraction (a) $\nu_f = 0.78$ (b) $\nu_f = 0.43$ and (c) $\nu_f = 0.12$

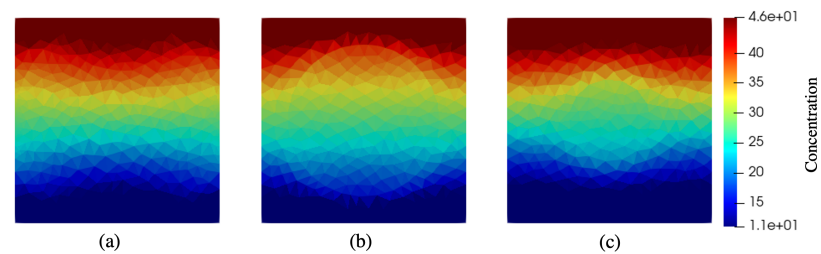


Figure 5.6: Concentration contour for a square unit cell matrix with an embedded circular filler inclusion for $\alpha = 1$ with different values for volume fraction (a) $\nu_f = 0.78$ (b) $\nu_f = 0.43$ and (c) $\nu_f = 0.12$

Figures 5.4, 5.5 and 5.6 illustrate the chemical potential, electric potential, and concentration contours respectively for all three different values of volume fraction of the filler, 0.78, 0.43 and 0.12 from (a) to (c) respectively under the same boundary conditions for

the unit cell in equilibrium situation ($\phi = 0$), where $\Delta\mu = 200 \times \mu_{\text{ref}} = 100\text{eV}$ and $\Delta\xi = -\frac{\Delta\mu}{q} = -100\text{V}$. So as we can see in Figure 5.4 the maximum electric potential is reported 200 which is the value on the top boundary, and the minimum value for electric potential is reported 0 on the bottom boundary which satisfy the applied boundary conditions. Similarly in the electric potential contour presented in Figure 5.5 the top boundary electric potential is -200 and the bottom boundary condition is 0 which satisfies the Dirichlet boundary condition applied on the unit cell for all three situations.

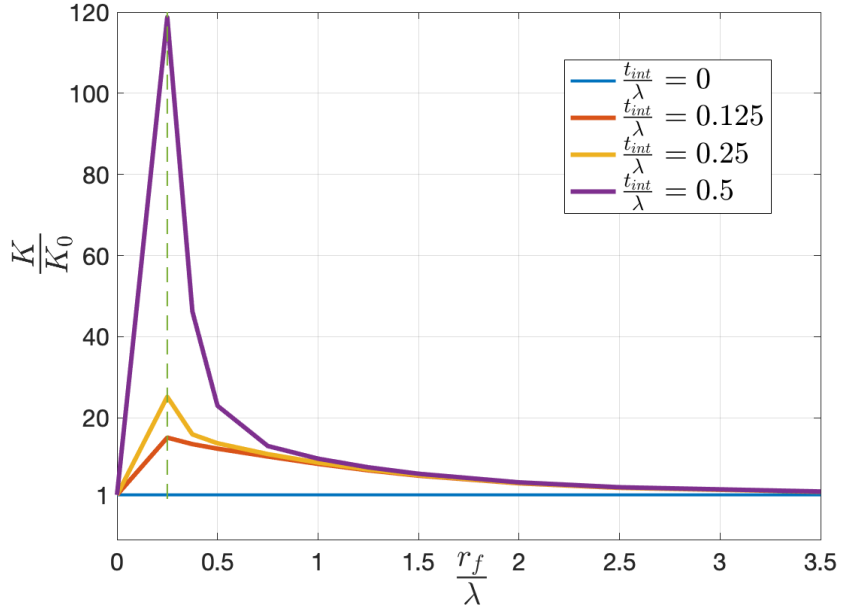


Figure 5.7: Normalized ionic conductivity versus the normalized radius of the circular inclusion in a constant volume fraction ($\nu_f = 0.2$) for different interphase thickness (t_{int}) from 0 to 2nm which is normalized with debye length ($\lambda_r = 4\text{nm}$).

In a battery like system the electrolyte is under a potential difference from the electrodes(anode and cathode), therefore as a result we can see in Figure 5.6 that the concentration in all three situation in a unit cell reached its maximum value, 4.6, at the point where the chemical potential is at its maximum value on the top boundary. Also the minimum concentration is reported exactly at the point we have the minimum chemical potential on the bottom boundary. Therefore the difference in effective conductivity in all these three situations is not the difference in maximum and minimum value of concentration, however, it is the result of concentration distribution and the difference in ion mobility of each layer

at each individual element in the whole domain.

Since we now have insight into the filler volume fraction at which the maximum ionic conductivity in a composite electrolyte is achieved, we can examine the effect of inclusion size. To that end, we assume a constant volume fraction of filler ($\nu_f = 0.2$) and vary the radius of the inclusion from 1nm to 14nm for four different interphase extension factors. Figure 5.7 illustrates the ionic conductivity of the composite with respect to the radius of the inclusion. For a given volume fraction, there is an optimal size and thus our model correctly resolves experimental observations that both an increase and decrease in ionic conductivity can occur with addition of fillers—the tuning of volume fraction and size is an important element to decide what behavior will be observed. We remark that for large inclusion size, we approach the matrix ionic conductivity ($\frac{K}{K_0} = 1$).

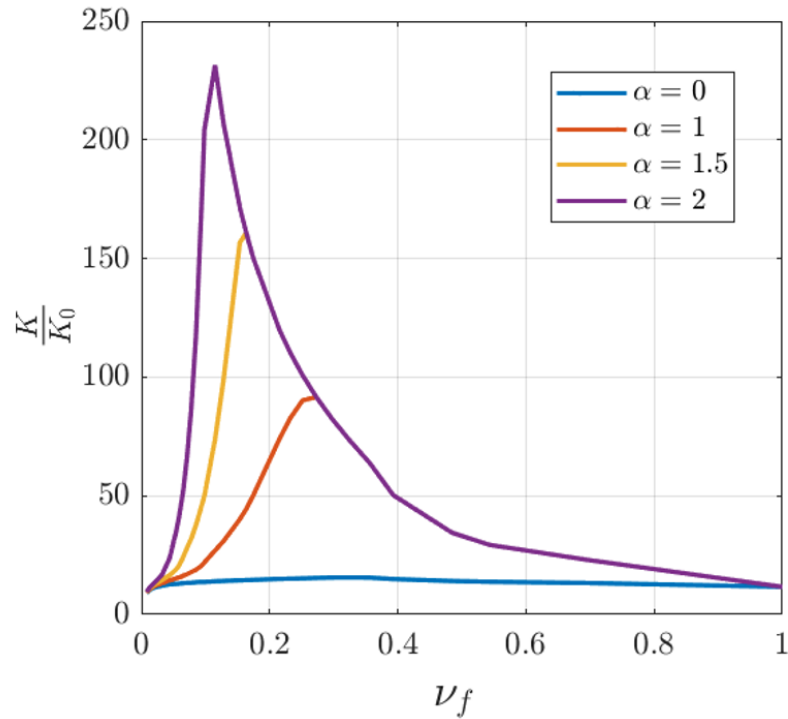


Figure 5.8: Normalized ionic conductivity with respect to the volume fraction of the elliptical filler for different interphase extension factors(α).

After solving the simplified model of circular shape filler in a square unit cell matrix, in another case study we consider an elliptical shape filler in a unit cell matrix where $a = 1\text{nm}$, $b = 0.5\text{nm}$ so the graph of normalized ionic conductivity vs volume fraction of

the filler is presented in Figure 5.8. The same trend for the effective ionic conductivity of the filler can be seen in this case study compared to simplified model in Figure 4.4. Which again says the maximum effective ionic conductivity can be reached at the point that we have the maximum amount of interphase with no polymer.

Comparing Figure 5.8 and Figure 4.4, we see that the maximum for elliptical fillers is higher compared to circular counterparts. the situation that we had circular filler inclusion. This prompts a closer examination fo ellipse aspect ratio. For that, we consider a square unit cell matrix with fixed $L = 10\text{nm}$ and elliptical inclusions with lengths a and b with interphase expansion factor of α .

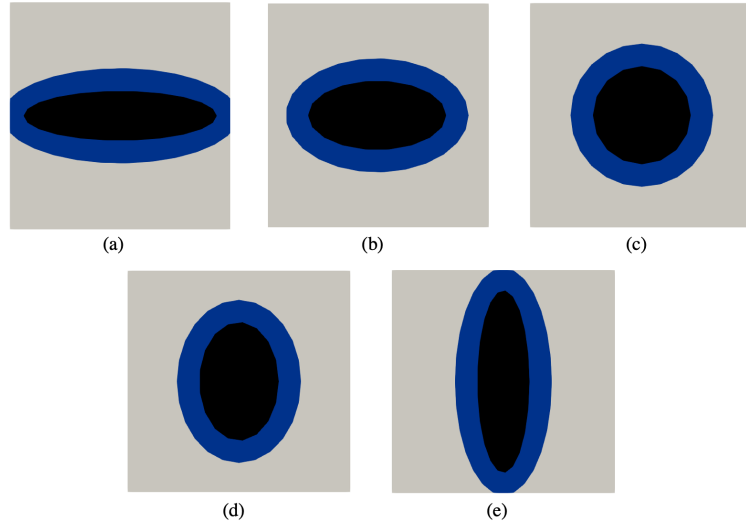


Figure 5.9: Schematics of a square unit cell matrix with an embedded elliptical inclusion with $\alpha = 1$ different $\frac{a}{b}$ (a)0.25 (b)0.5 (c)1 (d)1.5 (e)3.5

Figure 5.9 illustrates 5 different situations with different value of $\frac{a}{b}$ for $\alpha = 1$ in (a),(b),(c),(d) and (e) which represent 5 situations in a range of $\frac{a}{b}$ from 0+ up to 4. For instance, in Figure 5.9(a) we have a horizontal elliptical filler which is changing its shape to a a circular filler from (a) to (c) and then it becomes a vertical elliptical filler in (e).

Figure 5.10 illustrates the normalized ionic conductivity of the square unit cell matrix with an embedded elliptical filler with respect to the ratio $\frac{a}{b}$ of the elliptical filler for three different values of α with the same boundary conditions. We can conclude that as $\frac{a}{b}$ increases, the effective ionic conductivity of the composite get enhanced. Also as the interphase thickness (t_{int}) increases, the effect of $\frac{a}{b}$ becomes more pronounced.

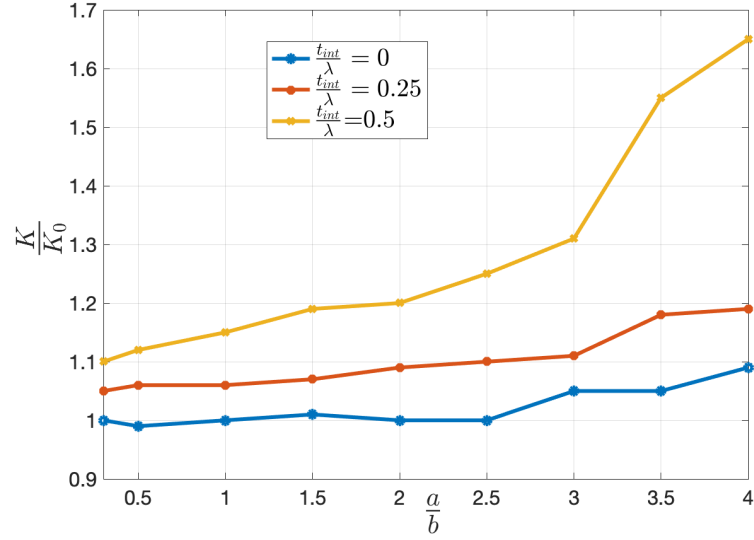


Figure 5.10: Normalized ionic conductivity with respect to $\frac{a}{b}$ for different interphase extension factor α . The ionic conductivity is normalized with the case of the $\alpha = 0$ and $\frac{a}{b} = 0.2$.

5.2 Effect of Deformation on Ionic Conductivity of an Electrolyte

In the previous sections the coupling between elasticity and electro-diffusion was neglected for simplicity and get a better insight about the problem. In this section for studying the effect of deformation on ionic conductivity of an electrolyte we consider a time-dependant fully-coupled electro-elasto-chemical system of equations presented in (2.22). As shown in Figure 5.11, an electrolyte is assumed to be stretched from two ends.

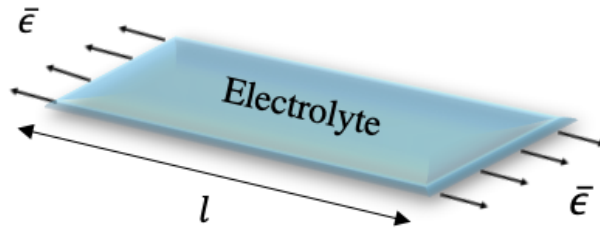


Figure 5.11: Schematic of a unit cell under a stretch of ϵ .

To study the effect of deformation on composite electrolytes, we consider a multi-layered

system as previously shown in Figure 4.3. Figure 5.12 illustrates the normalized ionic conductivity of a multi-layer composite electrolyte with respect to the applied strain for two different extension factors. The dashed lines show the case for small deformation while the solid lines are for the neo-Hookean elastically incompressible model. Clearly, deformation can significantly enhance ionic conductivity. The small deformation model predicts a linear relation between ionic conductivity and strain— also reported in experiments [31]. While, there is a departure from this linear relation at large strains, the deviation is perhaps not that high. We would, however, like to state that the polymer system examined in this work is not *too* soft. For softer materials (like gels) nonlinear deformation effects are likely to be more significant. Materials properties are considered as $\nu_f = 0.3$, $\alpha = 10^{-6} \times [80, 3, 3]$ and $Ey = [70, 0.03, 0.03]$ GPa.

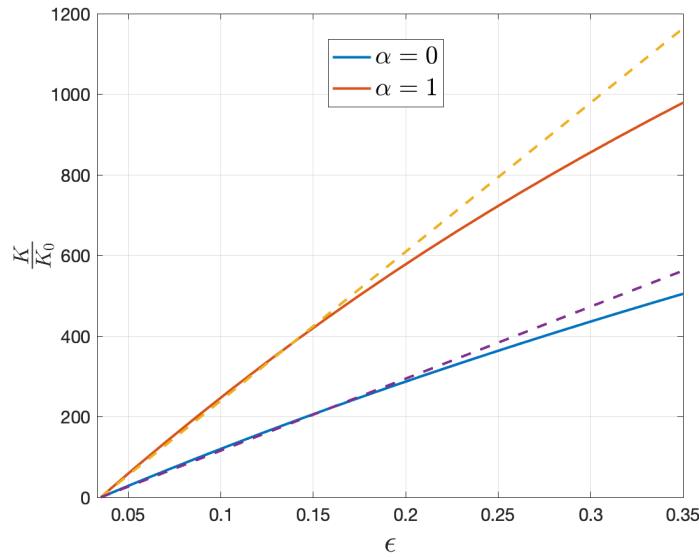


Figure 5.12: Normalized ionic conductivity versus average strain for different interphase extension factors α . The ionic conductivity is normalized with the case of the homogeneous system.

5.3 A Proposal for a Microstructure to Enhance Ionic Conductivity: Columnar Dielectric Spacers

In this section we, based on the insights at hand, we propose a novel microstructure that simply involves the addition of columnar dielectric spacer in parallel with the electrolyte in parallel—as shown in Figure 5.13. The key idea is that when we set columnar spacers parallel to electrolyte, the effective ionic resistance of the composite decreases to a smaller value. As shown in Figure 5.14, when we increase volume fraction of the dielectric spacers, the effective ionic conductivity can potentially increase by an order of magnitude. The addition of the dielectric in parallel with the electrolyte also helps enhance the electric field in the electrolyte which facilitates ion conduction. The compelling feature related to this microstructure is that it is very easy to fabricate.

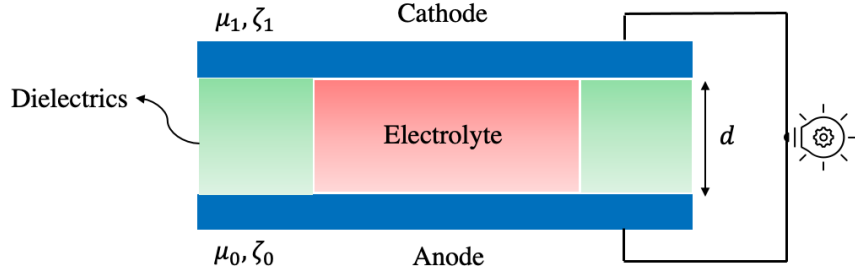


Figure 5.13: Schematic of a battery with an electrolyte and columnar dielectric spacers.

The governing equation for the electrostatics problem is as follows,

$$\begin{cases} -\lambda^2 \nabla^2 \zeta + \zeta = \frac{\phi}{q} & \text{in electrolyte,} \\ \nabla^2 \zeta = 0 & \text{in dielectrics.} \end{cases} \quad (5.1)$$

The inter-facial condition across the electrolyte-dielectric interfaces should be as follows,

$$[[\zeta]] = 0, \quad [[\epsilon \nabla \zeta]] \cdot n = 0. \quad (5.2)$$

Physically, the above inter-facial conditions means that there is no accumulation of free

charges on the interface, though the free charge density (per unit volume) may be nonzero in the electrolyte. Though the solution to (5.1), (5.2) may be complicated, from the linearity we observe that the electric potential difference should depend on $\Delta\phi$ linearly,

$$\Delta\zeta = \alpha_1\Delta\phi + \alpha_0. \quad (5.3)$$

Figure 5.14 illustrates the normalized ionic conductivity of a an electrolyte located between dielectric columnar spacers with respect to volume fraction of the columnar spacers. In this model the size of the electrolyte is constant and the size of dielectric increase from zero to infinity to have the range of volume fraction from 0 to 1. The graph shows enhancement in the ionic conductivity of the composite electrolyte by addition of dielectric columnar spacers and more importantly increase in the size of the spacers accelerate the enhancement of ionic conductivity in the electrolyte.

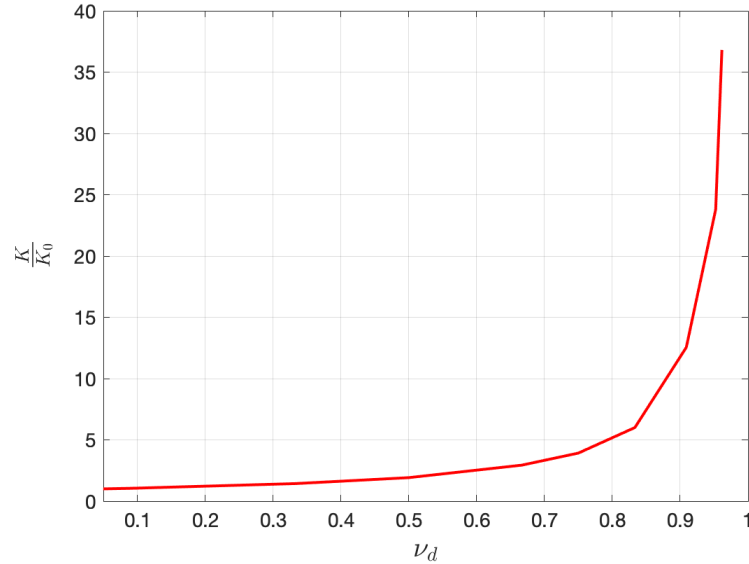


Figure 5.14: Normalized ionic conductivity with respect to the volume fraction of dielectric. $\frac{\gamma^{\text{dielectric}}}{\gamma^{\text{electrolyte}}} \approx 0$ the initial ionic concentration of the dielectric is considered as zero ($c_0^{\text{dielectric}} = 0$) while for electrolyte we have $c_0^{\text{electrolyte}} = 100 \frac{\text{mol}}{\text{m}^3}$.

Chapter 6

Concluding remarks

In this paper, we have presented a numerical implementation of the governing equations that dictate the electro-chemo-mechanical behavior of soft deformable solid electrolytes within an open-source finite element package *FEniCS*. The implementation is validated with known analytical solutions for some simplified cases. The numerical implementation allows us to design complex microstructures for the enhancement of ionic conductivity of solid electrolytes. Specifically, we were able to obtain insights into how the shape of embedded particles can influence the overall ionic conductivity of a composite electrolyte in addition to propose new types of microstructures to achieve this objective. A good future direction would be the use of topology optimization tools (including machine learning) to find optimal microstructures. With composite electrolytes, such as those discussed in this paper, durability of the chemo-mechanical-electrical system under cyclic loading such as discussed in other contexts also [52] is likely to become a significant issue.

References

- [1] A. K. Upadhyay and C. Reddy, "On the mechanism of charge transport in low density polyethylene," *Journal of Applied Physics*, vol. 122, no. 6, p. 064105, 2017.
- [2] S. Chu and A. Majumdar, "Opportunities and challenges for a sustainable energy future," *nature*, vol. 488, no. 7411, pp. 294–303, 2012.
- [3] R. Zito and H. Ardebili, *Energy Storage: A New Approach*. Wiley-Scrivener; 2 edition, 2019.
- [4] U. Kasavajjula, C. Wang, and A. J. Appleby, "Nano-and bulk-silicon-based insertion anodes for lithium-ion secondary cells," *Journal of power sources*, vol. 163, no. 2, pp. 1003–1039, 2007.
- [5] P. P. Prosini, M. Lisi, D. Zane, and M. Pasquali, "Determination of the chemical diffusion coefficient of lithium in lifepo4," *Solid State Ionics*, vol. 148, no. 1-2, pp. 45–51, 2002.
- [6] J. B. Goodenough and K.-S. Park, "The li-ion rechargeable battery: a perspective," *Journal of the American Chemical Society*, vol. 135, no. 4, pp. 1167–1176, 2013.
- [7] M. Winter and J. O. Besenhard, "Electrochemical lithiation of tin and tin-based intermetallics and composites," *Electrochimica Acta*, vol. 45, no. 1-2, pp. 31–50, 1999.
- [8] M. R. Lukatskaya, B. Dunn, and Y. Gogotsi, "Multidimensional materials and device architectures for future hybrid energy storage," *Nature communications*, vol. 7, no. 1, pp. 1–13, 2016.
- [9] K. Xu, "Electrolytes and interphases in li-ion batteries and beyond," *Chemical reviews*, vol. 114, no. 23, pp. 11503–11618, 2014.

- [10] S. A. Kumar and P. Kuppusami, “Enhancing the ionic conductivity in the ceria-based electrolytes for intermediate temperature solid oxide fuel cells,” in *Intermediate Temperature Solid Oxide Fuel Cells*, pp. 113–163, Elsevier, 2020.
- [11] K. Xu, “Nonaqueous liquid electrolytes for lithium-based rechargeable batteries,” *Chemical reviews*, vol. 104, no. 10, pp. 4303–4418, 2004.
- [12] H. Zhang, C. Li, M. Piszcz, E. Coya, T. Rojo, L. M. Rodriguez-Martinez, M. Armand, and Z. Zhou, “Single lithium-ion conducting solid polymer electrolytes: advances and perspectives,” *Chemical Society Reviews*, vol. 46, no. 3, pp. 797–815, 2017.
- [13] H. Kim, G. Jeong, Y.-U. Kim, J.-H. Kim, C.-M. Park, and H.-J. Sohn, “Metallic anodes for next generation secondary batteries,” *Chemical Society Reviews*, vol. 42, no. 23, pp. 9011–9034, 2013.
- [14] D. Aurbach, E. Zinigrad, Y. Cohen, and H. Teller, “A short review of failure mechanisms of lithium metal and lithiated graphite anodes in liquid electrolyte solutions,” *Solid state ionics*, vol. 148, no. 3-4, pp. 405–416, 2002.
- [15] S.-J. Tan, X.-X. Zeng, Q. Ma, X.-W. Wu, and Y.-G. Guo, “Recent advancements in polymer-based composite electrolytes for rechargeable lithium batteries,” *Electrochemical Energy Reviews*, vol. 1, no. 2, pp. 113–138, 2018.
- [16] S. Xu, Y. Zhang, J. Cho, J. Lee, X. Huang, L. Jia, J. A. Fan, Y. Su, J. Su, H. Zhang, and H. Cheng, “Stretchable batteries with self-similar serpentine interconnects and integrated wireless recharging systems,” *Nature communications*, vol. 4, no. 1, pp. 1–8, 2013.
- [17] H. Ardebili, “A perspective on the mechanics issues in soft solid electrolytes and the development of next-generation batteries,” *Journal of Applied Mechanics*, vol. 87, no. 4, 2020.
- [18] C. Tang, K. Hackenberg, Q. Fu, P. M. Ajayan, and H. Ardebili, “High ion conducting polymer nanocomposite electrolytes using hybrid nanofillers,” *Nano letters*, vol. 12, no. 3, pp. 1152–1156, 2012.

- [19] Q. Li, E. Wood, and H. Ardebili, "Elucidating the mechanisms of ion conductivity enhancement in polymer nanocomposite electrolytes for lithium ion batteries," *Applied Physics Letters*, vol. 102, no. 24, p. 243903, 2013.
- [20] G. S. MacGlashan, Y. G. Andreev, and P. G. Bruce, "Structure of the polymer electrolyte poly (ethylene oxide) 6: Liasf 6," *Nature*, vol. 398, no. 6730, pp. 792–794, 1999.
- [21] M. R. Johan, O. H. Shy, S. Ibrahim, S. M. M. Yassin, and T. Y. Hui, "Effects of al₂o₃ nanofiller and ec plasticizer on the ionic conductivity enhancement of solid peo–licf₃so₃ solid polymer electrolyte," *Solid State Ionics*, vol. 196, no. 1, pp. 41–47, 2011.
- [22] G. Hirankumar and N. Mehta, "Effect of incorporation of different plasticizers on structural and ion transport properties of pva-liclo₄ based electrolytes," *Heliyon*, vol. 4, no. 12, p. e00992, 2018.
- [23] S. Zhang, Z. Li, Y. Guo, L. Cai, P. Manikandan, K. Zhao, Y. Li, and V. G. Pol, "Room-temperature, high-voltage solid-state lithium battery with composite solid polymer electrolyte with in-situ thermal safety study," *Chemical Engineering Journal*, vol. 400, p. 125996, 2020.
- [24] W. Liu, N. Liu, J. Sun, P.-C. Hsu, Y. Li, H.-W. Lee, and Y. Cui, "Ionic conductivity enhancement of polymer electrolytes with ceramic nanowire fillers," *Nano letters*, vol. 15, no. 4, pp. 2740–2745, 2015.
- [25] Y.-J. Wang, Y. Pan, and D. Kim, "Conductivity studies on ceramic li₁. 3al₀. 3ti₁. 7 (po₄) 3-filled peo-based solid composite polymer electrolytes," *Journal of power sources*, vol. 159, no. 1, pp. 690–701, 2006.
- [26] F. Croce, G. Appetecchi, L. Persi, and B. Scrosati, "Nanocomposite polymer electrolytes for lithium batteries," *Nature*, vol. 394, no. 6692, pp. 456–458, 1998.
- [27] J. Weston and B. Steele, "Effects of inert fillers on the mechanical and electrochemical properties of lithium salt-poly (ethylene oxide) polymer electrolytes," *Solid State Ionics*, vol. 7, no. 1, pp. 75–79, 1982.

- [28] G. Liang, J. Xu, W. Xu, X. Shen, H. Zhang, and M. Yao, “Effect of filler-polymer interactions on the crystalline morphology of peo-based solid polymer electrolytes by y2o3 nano-fillers,” *Polymer Composites*, vol. 32, no. 4, pp. 511–518, 2011.
- [29] M. Dirican, C. Yan, P. Zhu, and X. Zhang, “Composite solid electrolytes for all-solid-state lithium batteries,” *Materials Science and Engineering: R: Reports*, vol. 136, pp. 27–46, 2019.
- [30] F. Larcht’e and J. Cahn, “The effect of self-stress on diffusion in solids,” *Acta Metallurgica*, vol. 30, no. 10, pp. 1835–1845, 1982.
- [31] T. Kelly, B. M. Ghadi, S. Berg, and H. Ardebili, “In situ study of strain-dependent ion conductivity of stretchable polyethylene oxide electrolyte,” *Scientific reports*, vol. 6, no. 1, pp. 1–9, 2016.
- [32] K. Mozaffari, L. Liu, and P. Sharma, “Theory of soft solid electrolytes: Overall properties of composite electrolytes, effect of deformation and microstructural design for enhanced ionic conductivity,” *Journal of the Mechanics and Physics of Solids*, p. 104621, 2021.
- [33] Y. Xiao and K. Bhattacharya, “A continuum theory of deformable, semiconducting ferroelectrics,” *Archive for Rational Mechanics and Analysis*, vol. 189, no. 1, pp. 59–95, 2008.
- [34] W. Hong, X. Zhao, and Z. Suo, “Large deformation and electrochemistry of polyelectrolyte gels,” *Journal of the Mechanics and Physics of Solids*, vol. 58, no. 4, pp. 558–577, 2010.
- [35] X. Wang and W. Hong, “Theory of ionic polymer conductor network composite,” *Applied Physics Letters*, vol. 98, no. 8, p. 081910, 2011.
- [36] E. Rejovitzky, C. V. Di Leo, and L. Anand, “A theory and a simulation capability for the growth of a solid electrolyte interphase layer at an anode particle in a li-ion battery,” *Journal of the Mechanics and Physics of Solids*, vol. 78, pp. 210–230, 2015.

- [37] D. Grazioli, O. Verners, V. Zadin, D. Brandell, and A. Simone, “Electrochemical-mechanical modeling of solid polymer electrolytes: Impact of mechanical stresses on li-ion battery performance,” *Electrochimica Acta*, vol. 296, pp. 1122–1141, 2019.
- [38] H. Zhang, M. Dehghany, and Y. Hu, “Kinetics of polyelectrolyte gels,” *Journal of Applied Mechanics*, vol. 87, no. 6, p. 061010, 2020.
- [39] M. Ganser, F. E. Hildebrand, M. Kamlah, and R. M. McMeeking, “A finite strain electro-chemo-mechanical theory for ion transport with application to binary solid electrolytes,” *Journal of the Mechanics and Physics of Solids*, vol. 125, pp. 681–713, 2019.
- [40] S. Narayan, E. M. Stewart, and L. Anand, “Coupled electro-chemo-elasticity: Application to modeling the actuation response of ionic polymer–metal composites,” *Journal of the Mechanics and Physics of Solids*, vol. 152, p. 104394, 2021.
- [41] J. Marshall and K. Dayal, “Atomistic-to-continuum multiscale modeling with long-range electrostatic interactions in ionic solids,” *Journal of the Mechanics and Physics of Solids*, vol. 62, pp. 137–162, 2014.
- [42] I. J. C. Sillamoni and M. I. Idiart, “A model problem concerning ionic transport in microstructured solid electrolytes,” *Continuum Mechanics and Thermodynamics*, vol. 27, no. 6, pp. 941–957, 2015.
- [43] L. Liu and P. Sharma, “Emergent electromechanical coupling of electrets and some exact relations—the effective properties of soft materials with embedded external charges and dipoles,” *Journal of the Mechanics and Physics of Solids*, vol. 112, pp. 1–24, 2018.
- [44] Q. Deng, L. Liu, and P. Sharma, “Electrets in soft materials: Nonlinearity, size effects, and giant electromechanical coupling,” *Physical Review E*, vol. 90, no. 1, p. 012603, 2014.
- [45] P. Sharma, S. Ganti, and N. Bhate, “Effect of surfaces on the size-dependent elastic state of nano-inhomogeneities,” *Applied Physics Letters*, vol. 82, no. 4, pp. 535–537, 2003.

- [46] P. Sharma and S. Ganti, “Size-dependent eshelby’s tensor for embedded nano-inclusions incorporating surface/interface energies,” *J. Appl. Mech.*, vol. 71, no. 5, pp. 663–671, 2004.
- [47] K. Mozaffari, S. Yang, and P. Sharma, “Surface energy and nanoscale mechanics,” *Handbook of Materials Modeling: Applications: Current and Emerging Materials*, pp. 1949–1974, 2020.
- [48] P. Sharma, “Size-dependent elastic fields of embedded inclusions in isotropic chiral solids,” *International Journal of Solids and structures*, vol. 41, no. 22-23, pp. 6317–6333, 2004.
- [49] X. Zhang and P. Sharma, “Inclusions and inhomogeneities in strain gradient elasticity with couple stresses and related problems,” *International Journal of Solids and Structures*, vol. 42, no. 13, pp. 3833–3851, 2005.
- [50] S. Natarajan and R. K. Annabattula, “A fenics implementation of the phase field method for quasi-static brittle fracture,” *Frontiers of Structural and Civil Engineering*, vol. 13, no. 2, pp. 380–396, 2019.
- [51] M. Siekierski, W. Wiecek, and K. Nadara, “Mesoscale models of conductivity in polymeric electrolytes—a comparative study,” *Electrochimica acta*, vol. 53, no. 4, pp. 1556–1567, 2007.
- [52] A. Dasgupta, P. Sharma, and K. Upadhyayula, “Micro-mechanics of fatigue damage in pb-sn solder due to vibration and thermal cycling,” *International Journal of damage mechanics*, vol. 10, no. 2, pp. 101–132, 2001.

Appendix

Implementation in *Python*

FEniCS is an open-source program environment for solving ordinary and partial differential equations automating central aspects of the finite element method. *FEniCS* uses the UFL (Unified Form Language) which takes a variational problem as an input together with a set of finite elements and generates low-level code for the automatic computation of the discrete system of equations. UFL is a domain-specific language embedded in Python for specifying finite element discretizations of differential equations in terms of finite element variational forms.

DOLFIN is a C++/Python library that functions as the main user interface of *FEniCS*. A large part of the functionality of *FEniCS* is implemented as part of *DOLFIN*. It provides a problem solving environment for models based on partial differential equations and implements core parts of the functionality of *FEniCS*, including data structures and algorithms for computational meshes and finite element assembly. To provide a simple and consistent user interface, *DOLFIN* wraps the functionality of other *FEniCS* components and external software, and handles the communication between these components [?]. In this project we implement *FEniCS* in using *DOLFIN* in *Python*, therefore we first need to import *DOLFIN* package as shown below.

```
from dolfin import *
```

In the first step of coding we need to define the domain. In every problem we solved in this project we consider a main-domain as the unit cell and the specify the filler and the interphase as the subdomains. The code below shows the way to specify a multi layer composite electrolyte. `rectangle3` represents the filler, `rectangle2` represents the whole filler and interphase, and the `rectangle1` represents the whole unit cell including the filler, interphase and polymer.

```
rectangle_1 = Rectangle(Point(0.0, 0.0), Point(Lx, Ly))
```

```

rectangle_2 = Rectangle(Point(0.0, 0.0), Point(Lx, L2))
rectangle_3 = Rectangle(Point(0.0, 0.0), Point(Lx, L1))
domain = rectangle_1
domain.set_subdomain(1, rectangle_3)
domain.set_subdomain(2, rectangle_2 - rectangle_3)
domain.set_subdomain(3, rectangle_1 - rectangle_2)

```

Then, we import the mesh on the domain as

```

mesh = generate_mesh(domain, MeshResolution)

```

For applying boundary conditions we must specify the boundaries. We do this by defining several classes, one for each boundary condition, as presented below,

```

class Left(SubDomain):
    def inside(self, x, on_boundary):
        return on_boundary and abs(x[0] ) < DOLFIN_EPS

class Right(SubDomain):
    def inside(self, x, on_boundary):
        return on_boundary and abs(x[0] - Lx) < DOLFIN_EPS

class Bottom(SubDomain):
    def inside(self, x, on_boundary):
        return on_boundary and abs(x[1] ) < DOLFIN_EPS

class Top(SubDomain):
    def inside(self, x, on_boundary):
        return on_boundary and abs(x[1] - Ly) < DOLFIN_EPS

```

```

class Omega_down(SubDomain):
    def inside(self, x, on_boundary):
        return ( (x[1]-L1)<=DOLFIN_EPS)

class Omega_middle(SubDomain):
    def inside(self, x, on_boundary):
        return ( (x[1]-L2)<DOLFIN_EPS and (x[1]-L1)>-DOLFIN_EPS )

class Omega_up(SubDomain):
    def inside(self, x, on_boundary):
        return ( (x[1]-L2)>-DOLFIN_EPS)

```

We create a MeshFunction to store the numbering of the subdomains. When creating a MeshFunction an argument specifying the type of the MeshFunction must be given. Allowed types are 'int', 'size_t', 'double' and 'bool',

```

subdomains = MeshFunction("size_t", mesh, 2, mesh.domains())
markers = MeshFunction('size_t', mesh, 2, mesh.domains())

subdomain_down = Omega_down()
subdomain_middle = Omega_middle()
subdomain_up = Omega_up()
subdomain_down.mark(markers, 0)
subdomain_middle.mark(markers, 1)
subdomain_up.mark(markers, 2)

```

To specify the weak form of the problem in *FEniCS*, we need to specify the function space V along with a set of test functions ($u, zeta, mu$) and trial functions (v_u, v_{zeta}, v_{mu}). To specify the function space as the parameters are not all of the same type, we need to specify each parameter first. For displacement we need a vector element with 2 components

(V_1) and for electric potential and chemical potential we simply need a finite element with only one component (V_1 and V_2) as shown below,

```
V1 = VectorElement('CG', mesh.ufl_cell(), 2)
V2 = FiniteElement('CG', mesh.ufl_cell(), 1)
V3 = FiniteElement('CG', mesh.ufl_cell(), 1)
V = FunctionSpace(mesh, MixedElement([V1, V2, V3]))
vtest = TestFunction(V)
duinc = TrialFunction(V)
up = Function(V)
(u,zeta, mu)=split(up)
(v_u,v_zeta,v_mu)=split(vtest)
```

where "CG" stands for Continuous Galerkin, implying the standard Lagrange family of elements. Instead of "CG", we could have written "Lagrange".

To differentiate the material properties for each subdomain and constant coefficient in each layer we wrote the following class,

```
class MaterialProperty3Layers(UserExpression):
def __init__(self, markers,L1_property,L2_property,L3_property, **kwargs):
    super().__init__(**kwargs)
    self.markers = markers

    self.L1_property = L1_property
    self.L2_property = L2_property
    self.L3_property = L3_property
def eval_cell(self, values, x, cell):
    if self.markers[cell.index] == 0:
        values[0] = self.L1_property
    elif self.markers[cell.index] == 1:
        values[0] = self.L2_property
    elif self.markers[cell.index] == 2:
```

```

        values[0] = self.L3_property
    else:
        values[0] = 1E+50

q = MaterialProperty3Layers(markers, q_1, q_2,q_3, degree=0)
E = MaterialProperty3Layers(markers, E_1, E_2,E_3, degree=0)
nu = MaterialProperty3Layers(markers, nu_1, nu_2,nu_3, degree=0)
C_0 = MaterialProperty3Layers(markers, C0_1, C0_2, C0_3, degree=0)
mu_h = MaterialProperty3Layers(markers, mu_h_1, mu_h_2, mu_h_3, degree=0)
ep_r = MaterialProperty3Layers(markers, ep_1, ep_2,ep_3, degree=0)
alpha = MaterialProperty3Layers(markers, alpha_1, alpha_2,alpha_3, degree=0)
beta = MaterialProperty3Layers(markers, beta_1, beta_2, beta_3, degree=0)
Gamma = MaterialProperty3Layers(markers, Gamma_1, Gamma_2, Gamma_3, degree=0)
G = MaterialProperty3Layers(markers, G_1, G_2,G_3, degree=0)
lmbda = MaterialProperty3Layers(markers, lmbda_1, lmbda_2, lmbda_3, degree=0)

```

The Dirichlet boundary conditions for all three main parameters(displacement, electric potential, chemical potential) are defined with the normalized values as follows,

```

bcb_disp = DirichletBC(V.sub(0), Constant((0.0,0.0)), Bottom() )
bcb_zeta = DirichletBC(V.sub(1), Constant(0.0), Bottom() )
bcb_mu = DirichletBC(V.sub(2), Constant(0.0), Bottom() )
bct_zeta = DirichletBC(V.sub(1), Constant(-1.), Top() )
bct_mu = DirichletBC(V.sub(2), Constant(2.), Top() )
bct_disp = DirichletBC(V.sub(0), Constant((0.0,3.5)), Top() )
bcs = [bcb_zeta,bct_zeta, bct_disp, bcb_disp]

```

After defining the boundary conditions and the material properties, we need to write the dimensionless weak form coupled system of equations that we derived in section 3.3 as shown below,

```

#Define Sigma
sigma = 2.0*G_bar*sym(grad(u)) + lambda_bar * tr(grad(u))*Identity(2)
sigma_alpha = alpha_bar * GM_bar / beta_bar * (mu - mu_h_bar ) *Identity(2)
            - alpha_bar**2/beta_bar * tr(grad(u)) * Identity(2)
#Define Concentration
c_term = GM_bar / beta_bar * (mu - mu_h_bar) -
        tr(grad(u)) * alpha_bar / beta_bar + C_0_bar

Eq_1_coupling_term = - Q_bar**2/beta_bar * (mu-mu_h_bar) *v_zeta*dx +
                    alpha_bar *Q_bar**2/beta_bar/GM_bar * tr(grad(u))*v_zeta *dx
Eq_1 = -dot(-ep_r * grad(zeta),grad(v_zeta)) * dx + Eq_1_coupling_term
Eq_2 = inner(-sym(grad(v_u) ), sigma )*dx + inner(-grad(v_u), sigma_alpha)*dx
Eq_3 = dot(-grad(v_mu), -Gamma_bar * c_term * grad(mu+zeta))*dx

```

Then we simply solve the system of equations using the solve command and differentiate the solution for all the parameters as follows,

```

Func = Eq_1 + Eq_2 + Eq_3
solve(Func == 0, up, bcs,form_compiler_parameters=ffc_options,
      solver_parameters={"newton_solver":{"linear_solver" : 'mumps'}})
(u1,zeta1,mu1)=up.split()

```

For time dependant problems we need to add the time dependant term to the equations and put the solve command in a while loop and solve the system of equations for each time step. The total time is set as 0.1 seconds and each time step is set as 0.02.

```

t=0
Total_time = 0.10

dt = Constant((0.02))
time = dt(0)

```

```

while time<=Total_time:
t=t+1
Eq_3_time_dependent_term = GM_bar / beta_bar *(1.0/dt) * (mu - mu_old)
- (1.0/dt) ( tr(grad(u)) - tr(grad(u_old)) ) * alpha_bar / beta_bar
Func = Eq_1 + Eq_2 + Eq_3 - v_mu * Eq_3_time_dependent_term *dx
solve(Func == 0, up, bcs,form_compiler_parameters=ffc_options,
solver_parameters={"newton_solver":{"linear_solver' : 'mumps'}})
(u1,zeta1,mu1)=up.split()
time+= dt(0)
up_old.assign( up )
(u_old,zeta_old, mu_old)=split(up_old)

cbar_sln = 1 / beta_bar * (mu1 - mu_h_bar) - tr(grad(u1))
* alpha_bar / beta_bar + C_0_bar
c_dimensional = C_ref * cbar_sln
time+= dt(0)

```

After solving the problem and finding value for the main parameters including displacement, electric potential and chemical potential we can find the effective ionic conductivity of composite electrolyte as follows,

```

cbar_sln = 1 / beta_bar * (mu1 - mu_h_bar) -
tr(grad(u1)) * alpha_bar / beta_bar + C_0_bar
c_dimensional = C_ref * cbar_sln

K = (1/(Ly)* assemble(1/(Gamma*c_dimensional)*dx))**(-1)

```

